iScience

CellPress
OPEN ACCESS

Article

Benzyl isothiocyanate suppresses development of thyroid carcinoma by regulating both autophagy and apoptosis pathway

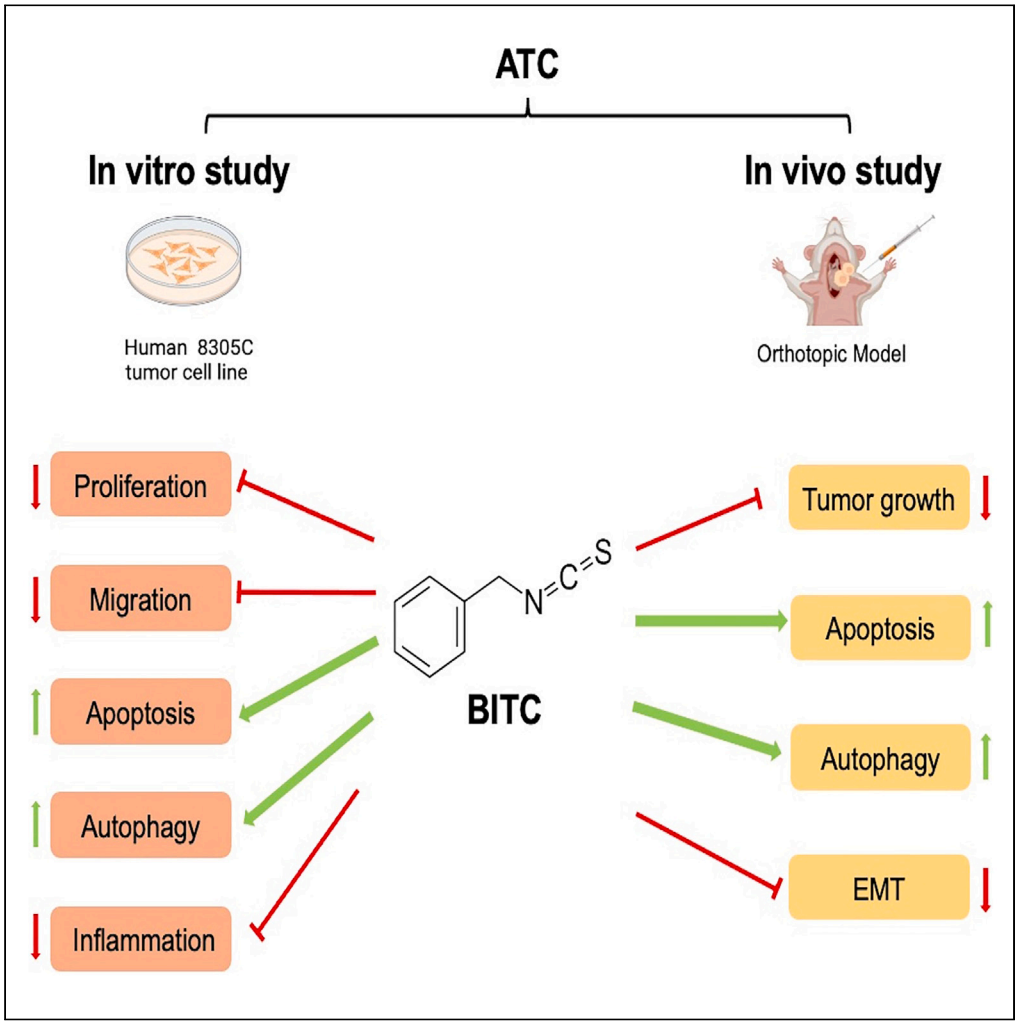

Rossella Basilotta, Giovanna Casili, Deborah Mannino, ..., Dorotea Sciacca, Emanuela Esposito, Irene Paterniti

emanuela.esposito@unime.it

Highlights

BITC treatment reduces ATC cell migration and proliferation *in vitro*

BITC reduces tumor growth on ATC orthotopic model *in vivo*

BITC acts by modulating autophagy, apoptosis, cell cycle, inflammation and EMT

BITC treatment reduces distant metastases

Basilotta et al., iScience 27, 110796
October 18, 2024
https://doi.org/10.1016/j.isci.2024.110796

iScience

CellPress
OPEN ACCESS

Article

Benzyl isothiocyanate suppresses development of thyroid carcinoma by regulating both autophagy and apoptosis pathway

Rossella Basilotta,[1] Giovanna Casili,[1] Deborah Mannino,[1] Alessia Filippone,[1] Marika Lanza,[1] Anna Paola Capra,[2] Domenico Giosa,[1] Stefano Forte,[3] Lorenzo Colarossi,[3] Dorotea Sciacca,[3] Emanuela Esposito,[1,4,*] and Irene Paterniti[1]

SUMMARY

Anaplastic thyroid carcinoma (ATC) is the most aggressive type of thyroid cancer, characterized by rapid growth and invasion and poor prognosis. Due to its rarity and aggressive nature, ATC is a difficult condition to treat, thus knowledge of the mechanisms underlying its progression represents important research challenges. Benzyl isothiocyanate (BITC) is a natural compound that has shown promising anticancer properties. The aim of this study was to evaluate the antitumor effect of BITC in ATC, highlighting signaling pathways involved in BITC mechanism of action. This work included *in vitro* and *in vivo* studies. Results obtained indicate that BITC, both *in vitro* and *in vivo*, has the potential to slow the progression of ATC through interactions with autophagy, reduction in epithelial-mesenchymal transition (EMT) and attenuation of inflammation. In conclusion, this study identifies BITC as a compound worth further investigation for the development of new treatment strategies for this aggressive form of thyroid cancer.

INTRODUCTION

Thyroid carcinomas (TCs) are the most frequent malignancy of the endocrine system and present a great variability in terms of molecular, cellular, and clinical characteristics. Based on these parameters, TCs are divided into differentiated carcinomas such as papillary thyroid carcinoma (PTC) and follicular thyroid carcinoma (FTC), characterized by a favorable prognosis, and undifferentiated carcinomas such as anaplastic thyroid carcinoma (ATC), lacking valid therapeutic possibilities.[1] This type of thyroid cancer typically arises from the follicular cells of the thyroid gland. It can develop *de novo* or may arise from pre-existing well-differentiated thyroid cancers, such as PTCs or FTCs.[2] ATC is a rare and highly aggressive form of thyroid cancer and accounts for only a small percentage of all thyroid cancer cases but is responsible for a disproportionate number of thyroid cancer-related deaths due to its aggressive nature and poor prognosis.[3] The incidence of this neoplasia is 3-fold higher in women and in individuals aged 25–65 years.[4] Diagnosis usually involves a combination of imaging studies; such as ultrasound, CT, or MRI (magnetic resonance imaging) scans; and a thyroid nodule biopsy, but because of its tendency to progress rapidly ATC is often diagnosed at an advanced stage making timely treatment difficult.[5] Conventional therapies, including surgery and radioactive iodine (RAI) treatment, often significantly prolong overall survival (OS) and progression-free survival (PFS) of patients with well-differentiated thyroid cancer (WDTC), while more invasive and metastatic anaplastic thyroid cancer often cannot be surgically removed and has poor response to local therapies. Anaplastic tumor cells are not responsive to radioiodine and most modalities of chemotherapy and radiotherapy.[6] While targeted therapies for ATC have evolved rapidly over the past decade, drug resistance is a major obstacle to improving the prognosis of patients with advanced thyroid cancer.[7]

Although many efforts have been made to improve the accuracy in the characterization of these tumors, the understanding of the mechanisms that regulate the differentiation of tumor cells and the identification of new therapeutic targets are important steps in the treatment of TCs. Most of the recently discovered targeted therapies for ATC inhibit the known oncogenic mechanisms in thyroid cancer initiation and progression such as mitogen-activated protein kinase (MAPK) pathway, PI3K/Akt-mTOR pathways, or VEGF (vascular endothelial growth factor).[8] Benzyl isothiocyanate (BITC), a bioactive natural product found in cruciferous vegetables, has shown anticancer effects through modulation of apoptosis, inflammation, and autophagic pathways. BITC has been shown to inhibit cancer progression in preclinical animal testing.[9–11] BITC is metabolized through degradation and hepatic conjugation by glutathione-S-transferase and glutamyl transpeptidase, respectively, and is 62% excreted in the urine as mercapturic acid.[12,13] Moreover, studies conducted on urine and plasma of healthy humans have confirmed the stability

[1]Departement of Chemical, Biological, Pharmaceutical and Environmental Sciences, University of Messina, Viale Ferdinando Stagno D'Alcontres 31, 98166 Messina, Italy
[2]Department of Clinical and Experimental Medicine, University of Messina, Viale Ferdinando Stagno D' Alcontres 31, 98166 Messina, ME, Italy
[3]Istituto Oncologico del Mediterraneo, Via Penninazzo 7, 95029 Viagrande, Italy
[4]Lead contact
*Correspondence: emanuela.esposito@unime.it
https://doi.org/10.1016/j.isci.2024.110796

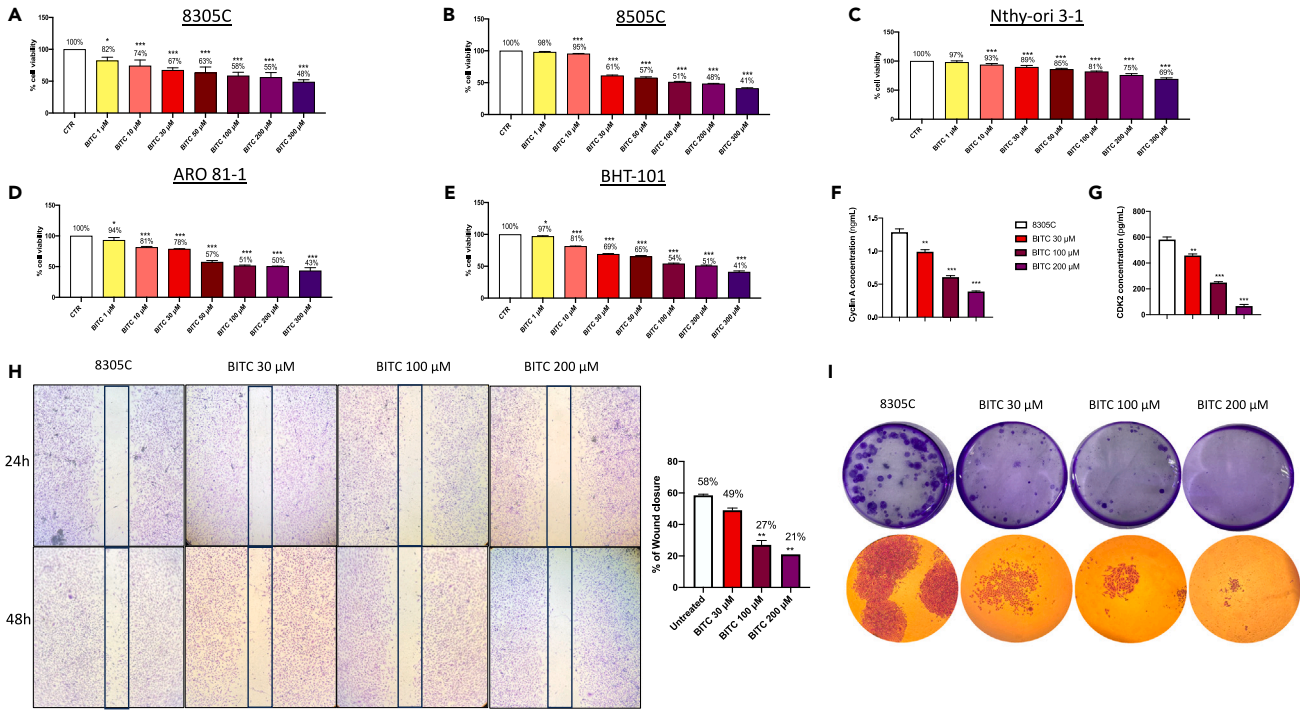

Figure 1. Effect of BITC on cell viability, cell cycle, cell migration, and colony formation

(A, B, D, and E) BITC treatment was able to significantly reduce cell viability in a concentration dependent manner on 8305C cells (A), 8505C cells (B), ARO 81-1 cells (D), and BHT-101 (E).

(C) A cytotoxic study of BITC effect on non-cancer thyroid cells were performed using Nthy-ori 3-1 cell line (C).

(F–H) The wound healing assay (scratch test) revealed a significant reduction in the number of cells migrating to the scratched area, following 48 h of BITC treatment at the concentrations of 100 µM and 200 µM (H); $^{**}p < 0.01$ vs. 8305C. ELISA assay revelated that BITC treatment induced cell-cycle arrest through the downregulation of CDK2 (F) and cyclin A (G); $^{**}p < 0.01$; $^{***}p < 0.001$ vs. 8305C.

(I) The colony formation assay of 8305C cells treated with 30 µM, 100 µM, and 200 µM BITC for 24 h, followed with 0.1% (w/v) crystal violet staining of attached cells after 10 days, showed a significant reduction of colonies formation compared to 8305C cells (I); $^{***}p < 0.001$. Data are representative of at least three independent experiments. Values are means ± SEM. We used one-way ANOVA test followed by Bonferroni post hoc test for multiple comparisons. $^{*}p < 0.05$ vs. CTR; $^{**}p < 0.01$ vs. CTR; $^{***}p < 0.001$ vs. CTR.

of intermediate metabolites of BITC produced during the mercapturic acid pathway, since only low levels of free BITC were detectable.[14] Some studies report the beneficial effect of BITC in the inhibition of both basal and hepatocyte growth factor (HGF)-stimulated migration and in the invasion of breast cancer cells, effects that seem to be attributable to urokinase-type plasminogen activator (uPA) downregulation and plasminogen activator inhibitor-1 (PAI-1) upregulation, which in turn may be mediated by suppression of Akt activation.[9] In addition, orthotopic xenograft models of breast cancer have documented the inhibition of EMT by BITC, through upregulation of adherent junction proteins (E-cadherin and occludin) and downregulation of mesenchymal markers such as vimentin and fibronectin and suppression of E-cadherin transcriptional repressors (snail and slug).[15] Further works showed that BITC treatment inhibited the expression of pro-survival proteins IGF1R, mammalian rapamycin kinase (mTOR), and FGFR3 by upregulation of miR-99a in bladder cancer cell lines, providing strong preclinical evidence for miRNA-based treatment of cancer.[16] The most reported signaling pathway with which BITC interacts is certainly autophagy. BITC is known to affect the mammalian target of rapamycin (TOR) pathway, which is a key regulator of autophagy, potentially affecting the balance between cell survival and cell death in cancer cells. BITC's ability to induce autophagy in cancer cells has led to research exploring its potential therapeutic applications. Some studies suggest that combining BITC with autophagy inhibitors or other cancer therapies could improve its effectiveness in treating certain types of cancer.[17,18] Research on BITC and autophagy has been conducted in various types of cancer, including breast cancer, prostate cancer, colon cancer, and more.[19–21] The specific effects of BITC on autophagy may vary depending on the type of cancer cell and context. BITC causes inhibition of cytoprotective autophagy of human gastric adenocarcinoma AGS cells by decreasing both autophagy initiator proteins and lysosomal degradation,[10] while it has demonstrated antitumor activity in human prostate cancer cells through the induction of early protective autophagy pathways by inhibiting mTOR signaling regardless of their sensitivity to androgens.[22] However little attention has been paid to the impact that BITC could have on the progression of thyroid cancer. The aim of this work was to evaluate, through both *in vitro* and *in vivo* models, the antitumor effect of BITC in ATC, highlighting signaling pathways involved in its mechanism of action.

This research aiming to evaluate the impact of BITC on ATC represents a significant effort to address a challenging and deadly cancer type. Understanding how BITC influences ATC progression and identifying relevant signaling pathways can potentially lead to the

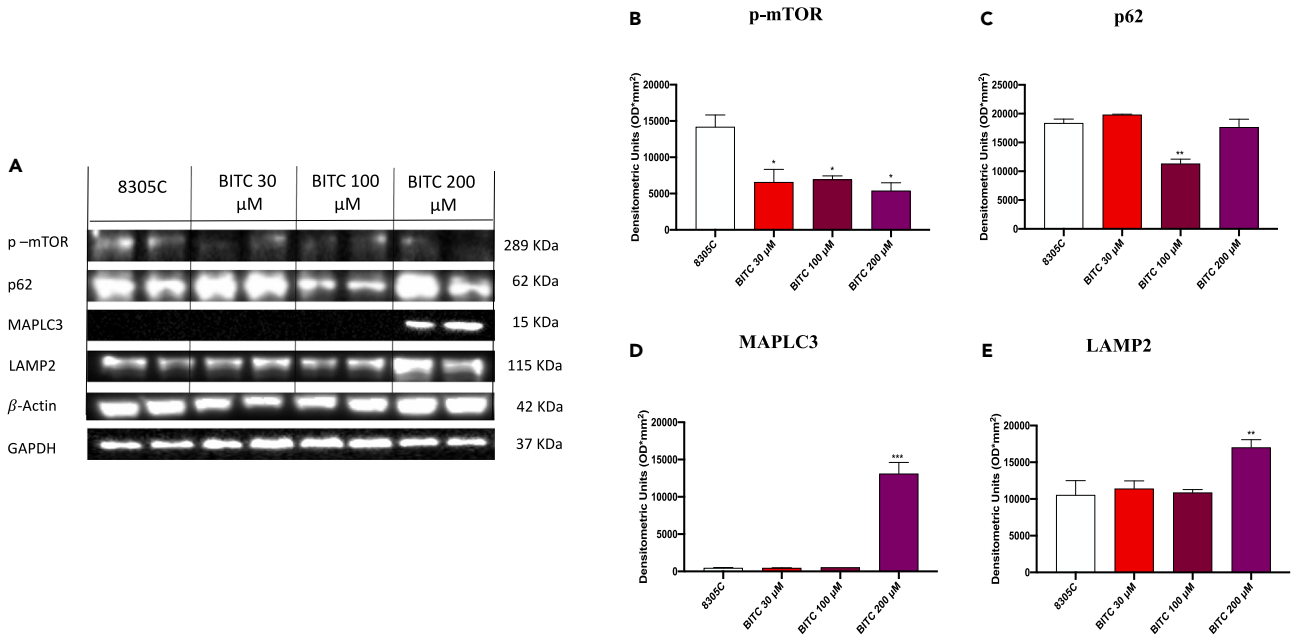

Figure 2. Effect of BITC on autophagy markers expression in 8305C cells

(A) The blots revealed a significant modulation of autophagy markers expression following BITC treatment.

(B) BITC at the concentrations of 30 μM, 100 μM, and 200 μM was able to significantly reduce the expression of p-mTOR. *$p < 0.05$ vs. 8305C.

(C) BITC at the concentration of 100 μM causes a significant reduction of p62 expression. **$p < 0.01$ vs. 8305C.

(D and E) Treatment with 200 μM BITC was also able to increase the expression of MAPLC3 (D) and LAMP2 (E) markers compared to 8305C cells; ***$p < 0.001$ vs. 8305C; **$p < 0.01$ vs. 8305C. Values are means ± SEM. We used one-way ANOVA test followed by Bonferroni post hoc test for multiple comparisons.

development of innovative and more effective therapeutic approaches for ATC patients, offering hope for improved outcomes and quality of life.

RESULTS

In vitro results

BITC reduces TC cell viability

MTT (3-(4,5-dimethylthiazol-2-yl)-2,5-diphenyltetrazolium bromide) assay was used to assess 8305C, 8505C, ARO 81-1 BHT-101, and Nthy-0ri-3-1 cell viability following 24 h of treatment with BITC at different concentrations (1, 10, 30, 50, 100, 200, and 300 μM). Our results show that BITC treatments were able to decrease cells viability in a concentration dependent manner as showed in Figures 1A–1C. Based on the cytotoxicity study that accurately determines the IC50 of BITC using MTT assay, showed in Figure S1A (IC50 = 147.4 μM), we decided to investigate in further analysis only BITC at concentrations of 30, 100, and 200 μM. Moreover, since BITC showed better effects on all cell lines, we decided to continue to investigate its effect on only the anaplastic carcinoma cell line, because it represents the most aggressive type of thyroid carcinoma with poor prognosis and with limited therapeutic possibilities.

BITC reduces cell migration and proliferation

The effect of BITC on 8305C cell migration was evaluated using an *in vitro* wound healing test. Confluent cells were scratched and then subjected to BITC treatment for 48 h. The images were acquired, and the percentage of cells migrated to the scratched area was calculated. Our results showed that BITC led to a marked reduction in the number of cells migrating to the scratched area, particularly at the concentration of 100 and 200 μM after 48 h of treatment (Figure 1D). The ability of 8305C cells to form colonies was evaluated following treatment with 30, 200, and 300 μM of BITC. The results of 0.1% (w/v) crystal violet staining suggested that BITC significantly inhibited colony formation (Figure 1E). Our findings also revealed the ability of BITC to induce cell-cycle arrest through the downregulation of CDK2 and cyclin A, suggesting a role in blocking the transition from G1 phase to S phase, but also G2 phase (data shown in Figures 1F and 1G).

BITC modulates autophagy markers

To examine the effect of BITC on the autophagy of 8305C cells, we measured the expression of autophagy-related proteins (p-mTOR, p62, MAP LC3, and LAMP2) by western blot analysis. Our data showed an increase expression of p-mTOR and p62 in 8305C cells that was significantly reduced after the treatment with 30, 100, and 200 μM BITC (Figures 2B and 2C). At the same time, we demonstrate a downregulation of MAP LC3 and LAMP2 in 8305C cells that was increased following the treatment with 200 μM BITC (Figures 2D and 2E).

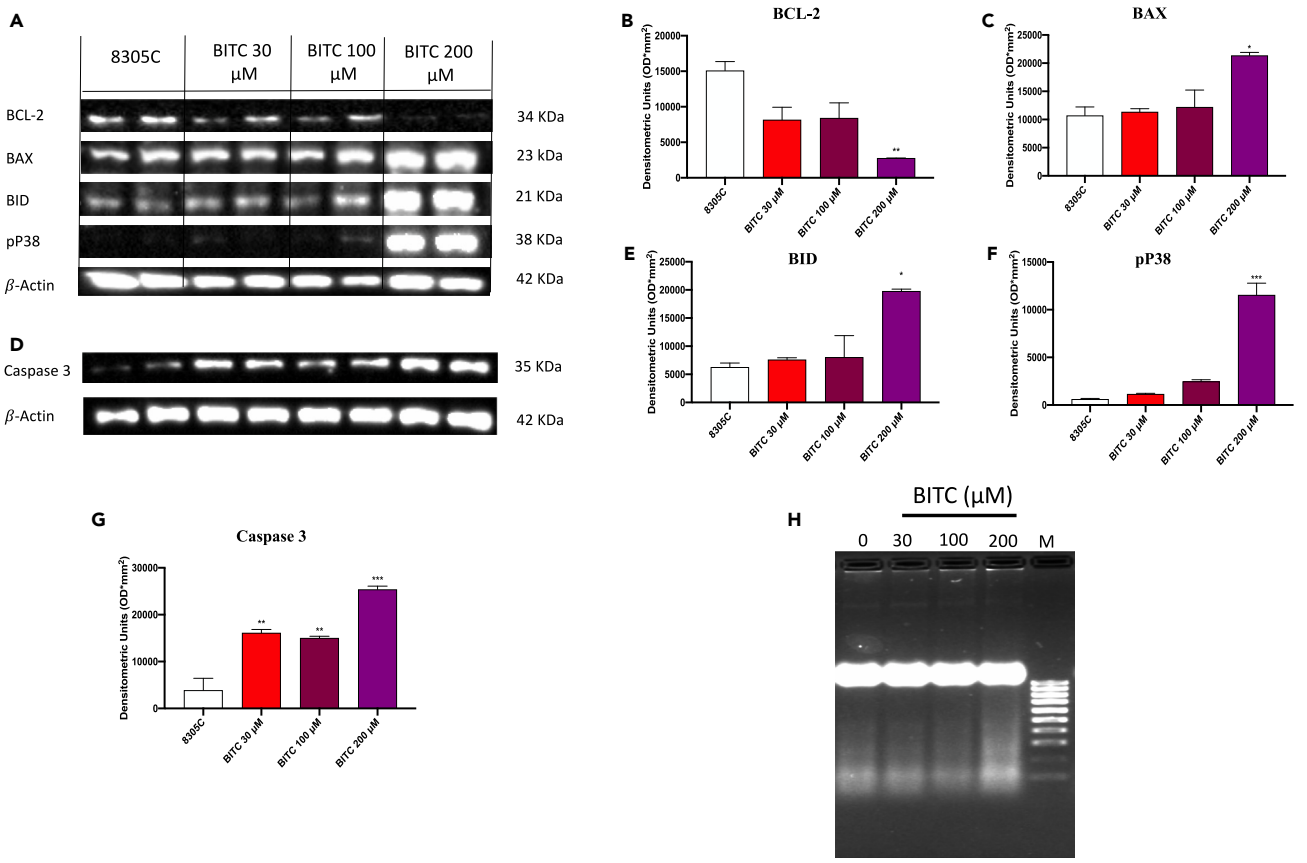

Figure 3. Effect of BITC on apoptosis markers expression in 8305C cells

(A) The blots revealed a significant modulation of apoptosis markers expression following BITC treatment.

(B and C) BITC at the concentration of 200 μM was able to significantly reduce the expression of BCL-2 (B) and to increase the expression of BAX (C).

(D–G) Caspase-3 (D), BID (E), and pP38 (F) markers compared to 8305C cells; ***$p < 0.001$ vs. 8305C; **$p < 0.01$ vs. 8305C; *$p < 0.05$ vs. 8305C.

(H) Values are means ± SEM. We used one-way ANOVA test followed by Bonferroni post hoc test for multiple comparisons. Fragmentations of genomic DNA in 8305C cells treated with BITC 30 μM, 100 μM, and 200 μM for 24 h. DNA laddering formation was viewed on ethidium bromide-stained gel (2%) and photographed by UV illumination. M, molecular weight marker.

BITC modulates apoptosis pathway

Western blot analysis was performed in order to evaluate the effect of BITC on the expression of apoptotic markers such as BAX, BID, BCL-2, and caspase-3. Our results showed that BITC, at higher concentrations of 200 μM, significantly improved the levels of pro-apoptotic proteins BAX and BID (Figures 3C–3E), and it was also able to reduce the expression of the anti-apoptotic BCL-2 protein (Figure 3B). In addition, BITC at the concentration of 200 μM was capable to induce the activation of p38 promoting 8305C cell death (Figure 3F). The induction of the apoptotic process was confirmed by the DNA fragmentation assay and is mediated by the activation of caspase-3. Our results showed that treatment with BITC significantly activated caspase-3 at all the concentrations (Figures 3D–3G). Following agarose gel electrophoresis of 8305C cells treated with BITC, a typical ladder pattern of internucleosomal fragmentation was observed in cells after 200 μM BITC treatment for 24 h (Figure 3H).

BITC modulates inflammation-associated cancer

Previous studies have indicated that cancer may be promoted and/or exacerbated by inflammation and infection. The cytokines produced by activated innate immune cells that stimulate tumor growth and progression are considered as important components in this process.[23] In this contest our data showed an important downregulation of TRAF6, IL-17, and IL-12p70 in 8305C cells after the treatment with BITC compared to the control (Figure 4.), suggesting its role in maintaining the tissue barrier functions necessary for host defense.

***In vivo* results**

BITC reduces tumor growth on ATC orthotopic model

To evaluate the effect of BITC on the growth of ATC cells *in vivo*, the 8305C orthotopic model was established in nude mice. Tumor progression was monitored through tumor size assessment showed in Figure S1C. The histological analysis of the ATC group showed

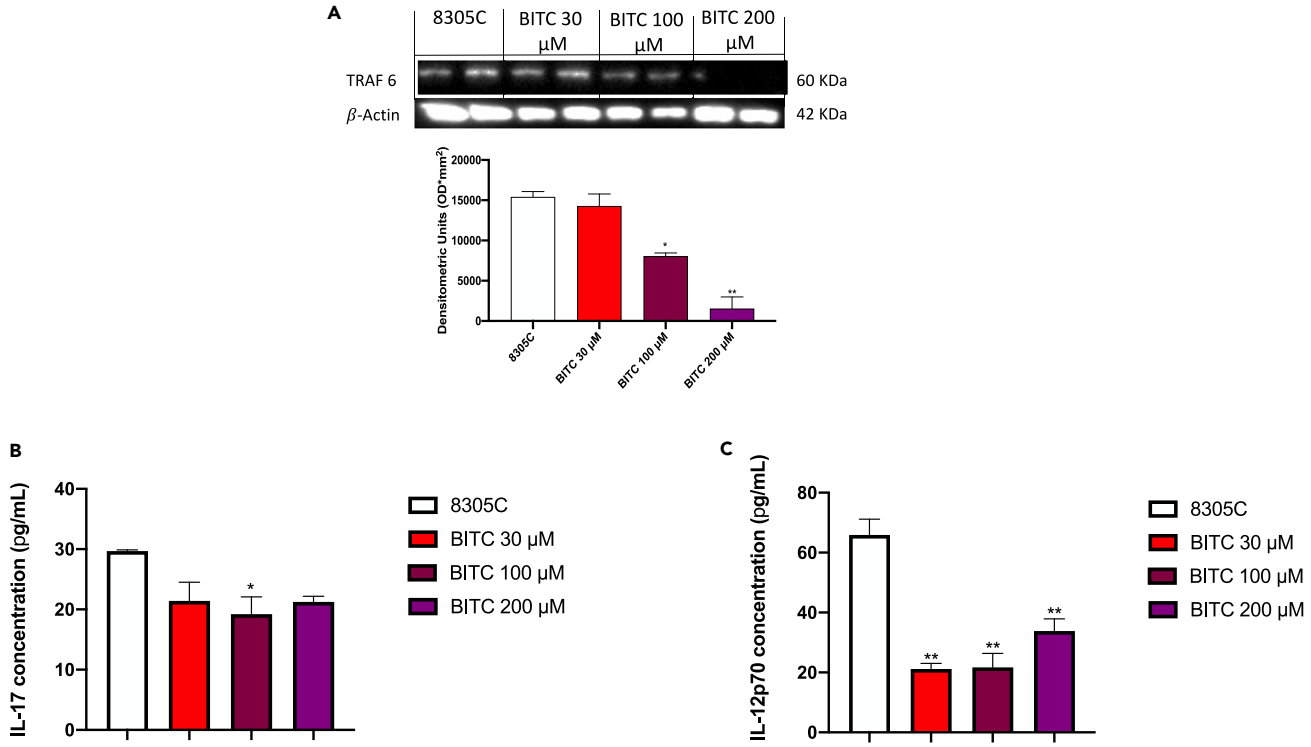

Figure 4. Effect of BITC on inflammation-associated cancer in 8305C cells

(A) BITC treatments at the concentrations of 100 μM and 200 μM was able to significantly reduce the expression of TRAF6, compared to 8305C cells. $^{**}p < 0.01$ vs. 8305C; $^{*}p < 0.05$ vs. 8305C.

(B and C) The enzyme-linked immunosorbent assay (ELISA) revealed a significant decrease of IL-12p70, following BITC treatments at all the concentrations (C) and of IL-17 levels, especially at the concentration of 100 μM (B) $^{*}p < 0.05$ vs. 8505C; $^{**}p < 0.01$ vs. 8305C. Values are means ± SEM. We used one-way ANOVA test followed by Bonferroni post hoc test for multiple comparisons.

features of a high-grade malignant neoplasm characterized by high-grade nuclear atypia, marked cellular pleomorphism, necrosis, and significant neutrophil infiltration compared to the sham group.[24] Our results demonstrate that the treatment with BITC at doses of 10 and 30 mg/kg was able to significantly reduce these pathological features as showed in Figure 5. BITC was able to significantly reduce tumor weight at all the doses (Figure S1D), while no important changes in the animals' body weight were shown during the experiments (Figure S1B).

BITC ameliorates the morphological aspects of ATC studied by Masson's trichrome staining

The morphology of orthotopic 8305C tumors was observed on histologic sections after Masson's trichrome staining. Overall, the presence of collagen fibers stained in blue around the tumors, as well as their invasion within the tumors are noticeable in the ATC group compared to sham group. Our data showed that BITC treatments at doses of 30 and 100 mg/kg were able to ameliorate these morphological aspects as shown in Figure 6.

BITC modulates EMT markers expression on ATC orthotopic tumor

EMT causes significant morphological changes from the epithelial to mesenchymal phenotype and promotes greater progression and invasion.[25] In this context, our results showed a significant upregulation of mesenchymal marker N-cadherin and a downregulation of epithelial factor E-cadherin in the ATC group compared to sham group (Figures 7B–7H). BITC treatments at doses of 30 and 100 mg/kg led to significant downregulation of N-cadherin expression and upregulation of E-cadherin expression in orthotopic tumors, carrying out an important role in reducing tumoral migration and invasion as shown in Figure 7. These results were confirmed by western blot analysis performed on the thyroid samples collected in the ATC orthotopic model (Figure 9).

BITC reduced S100 expression on ATC orthotopic tumor

S100A4 protein is also known as "metastasin," and its increased expression has been associated with many malignancies including thyroid cancer.[26–29] Expression of S100A4 is increased in ATC group compared to sham counterpart where expression is low or non-existent.

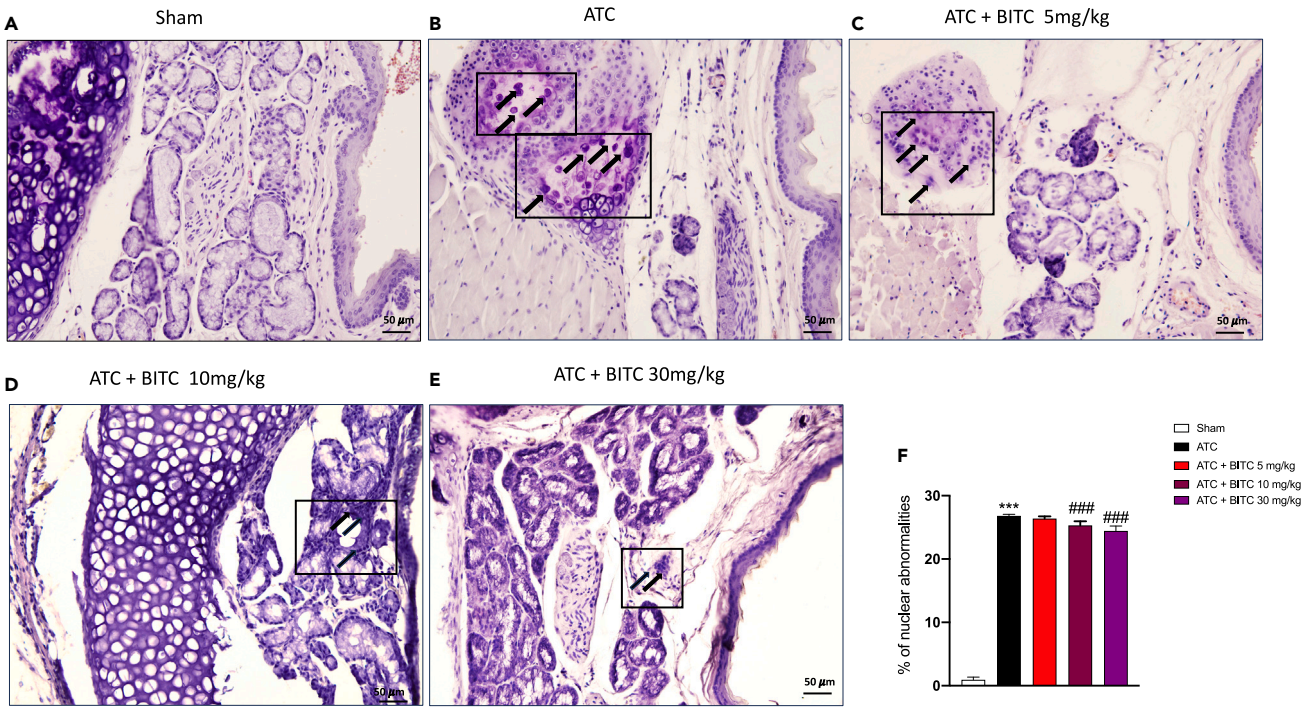

Figure 5. Effect of BITC on tumor growth in an orthotopic model of ATC

(A, D, and E) Hematoxylin and eosin staining revealed features of high grade neoplasm such as high-grade nuclear atypia, marked cellular pleomorphism, necrosis, and neutrophil infiltration in the ATC group (B) compared to the sham group (A). BITC treatments at the concentrations of 10 mg/kg (D) and 30 mg/kg (E) were able to reduce these features compared to the ATC group (B). BITC treatment at the dose of 5 mg/kg (C) did not demontrate a significant effect.

(F) Quantification of nuclear morphology changes after treatment with BITC. The data are representative of at least three independent experiments. The sections were observed and photographed at 20× magnification.

Expression of S100A4 has been shown to be inversely related to E-cadherin expression in some cancers, leading to a more aggressive phenotype and hence a worse prognosis. BITC treatments mainly at doses of 30 mg/kg and 100 mg/kg were able to reduce S100 expression compared to the ATC group as shown in Figure 8. These results were confirmed by western blot analysis performed on the thyroid samples collected in the ATC orthotopic model (Figure 9).

BITC reduced lung metastases

The lungs are the most common distant metastatic site of ATC and the metastases are almost always not surgically resectable.[30] Since ATC tends to metastasize rapidly, we evaluated the effect of BITC in reducing lung metastases. The histological evaluation showed that BITC at doses of 10 mg/kg and 30 mg/kg significantly reduced the diffuse tumor cell infiltration as well as the presence of multifocal cellular aggregates in lung tissues compared to the ATC group (Figure 10).

BITC modulated apoptotic and autophagy pathways in ATC

To confirm the key role of autophagy in the progression of ATC, we evaluated some of the main autophagy markers by western blot analysis, also on the thyroid samples collected in the ATC orthotopic model. The results showed thatBITC was able to significantly increase the expression of PTEN, and reduce the expression of p-mTOR, p62 and SOS-1 mainly at the doses of 30 and 100 mg/kg compared to ATC group, as showed in Figure 11. For the same reason we also investigated the expression of apoptotic factors, demonstrating that BITC was able to significantly increase the expression of BID and BAD expression and reduce BCL-2 expression, mainly at the highest doses as showed in Figure 12.

DISCUSSION

Although ATC is the type of thyroid cancer with the lowest incidence, compared to differentiated carcinomas, it is characterized by a high risk of recurrence and poor prognosis.[31] Conventional treatments including surgery and chemotherapy have proven ineffective for ATC and have failed to improve survival rates.[32] Accumulating evidence suggests that autophagy plays a key role in thyroid cancer, acting to promote tumor cell viability and metastatic disease through maintenance of cancer stem cells (CSCs), supporting epithelial-to-mesenchymal transition (EMT), and preventing tumor cell death.[33] Autophagy refers to the process of maintaining cellular homeostasis by which dysfunctional cellular

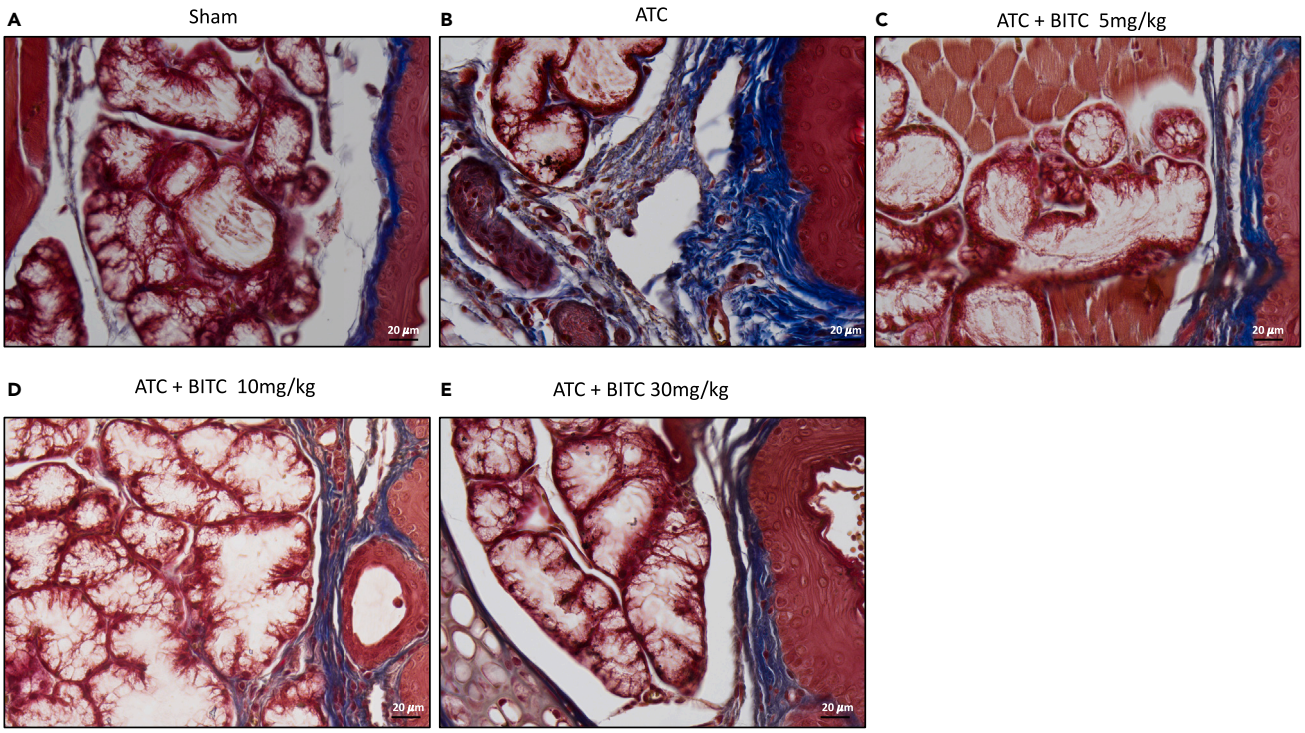

Figure 6. Effect of BITC on tumor morphology in an orthotopic model of ATC

Masson's trichrome staining of ATC (8305C) tumors developed in nude mice orthotopically; cytoplasm is stained in red; the collagen is stained in blue. Sham group (A); ATC group (B); BITC groups (C–E). The data are representative of at least three independent experiments. The sections were observed and photographed at 40× magnification.

components, such as damaged proteins or aging organelles, are recruited directly into lysosomes via autophagic vacuoles for degradation.[34] Several signaling pathways participate in autophagy formation, including PI3K/Akt/mTOR pathways, MAPK, and AMP-activated protein kinase (AMPK), with PI3K/Akt/mTOR signaling reported more. In the PI3K-AKT-mTOR pathway, mutations of PIK3CA, PTEN, and AKT1 were detected in patients with ATC. PTEN (phosphatase and tensin homolog) encoded PTEN enzyme, which acts as a tumor suppressor by regulating cell division and preventing abnormal cell growth and division.[35] mTOR is a regulatory protein, involved in the PI3K/Akt/mTOR pathway, which increases the uptake of iodine from thyroid cells to promote cell proliferation and survival. Genetic alterations occurring in this pathway play a role in the progression of ATC. mTOR is a highly attractive target via several therapeutic strategies.[36–38] mTOR interacts with the adaptor protein p62 (also known as sequestosome-1, SQSTM-1, or A170) in the formation of the complex in the lysosomal compartment. P62 is a crucial molecule in the regulation of cell growth, survival, and proliferation. P62 recognizes polyubiquitin chains through its C-terminal domain and binds to LC3, thus promoting autophagic degradation of ubiquitinated loads. P62 colocalized with LAMP2 (a lysosomal marker) and Rags and the translocation of the mTORC1 complex to the lysosomal surface is necessary for the interaction of mTOR.[39] Another process that can indirectly influence autophagy is the activation of the Ras-MAPK pathway, mediated by SOS1 (son of sevenless homolog 1). SOS1 participates in the transduction of signals from growth factor receptors and may respond to stressors such as oxidative stress or DNA damage, which can trigger autophagic responses as a means of removing damaged cellular components and promoting cell survival. Activating Ras can, in fact, activate the mTOR path, which is a key negative regulator of autophagy.[40] Our results showed that BITC was able to increase the expression of the tumor suppressor gene PTEN, leading to the modulation of the autophagic pathway mediated by downregulation of p-mTOR, P62, and SOS1 and upregulation of LC3 and LAMP2, contributing to the improvement of apoptosis and repression of ATC cell proliferation and invasion. Autophagy influences cancer progression, supports cell survival under stress within tumors and drives cell death, impacting tumor growth.[41] These results are consistent with the literature as BITC has been shown in several types of cancer to reduce cell viability and proliferation through modulation of autophagic processes. An example is the antiproliferative action shown by BITC by processing the autophagy-related LC3-II protein in Rv1 and PC3 prostate cancer cells by inhibiting the mTOR signaling pathway.[22] Similar effects were reported in human colorectal carcinoma HCT-116 cells, where BITC upregulated autophagy symbol proteins, including LC3BII and LAMP1.[18] Likewise, induction of autophagy by BITC was demonstrated in A549, H661, and SK-MES-1 lung cancer cell lines, through accumulation of LC3-II protein and increased expression of Atg5, which led to inhibition of tumor growth.[17] Also in breast cancer cells MDA-MB-231, MCF-7, MDA-MB-468, BT-474, and BRI-JM04, BITC was able to activate autophagy both *in vitro* and *in vivo* by LC3 cleavage and suppression of p62 and mTOR expression.[42] The activation of apoptotic processes has been confirmed by our data obtained both *in vitro* and *in vivo* through the increase in the expression of proapoptotic markers such as BID, BAX, and BAD and the decrease of

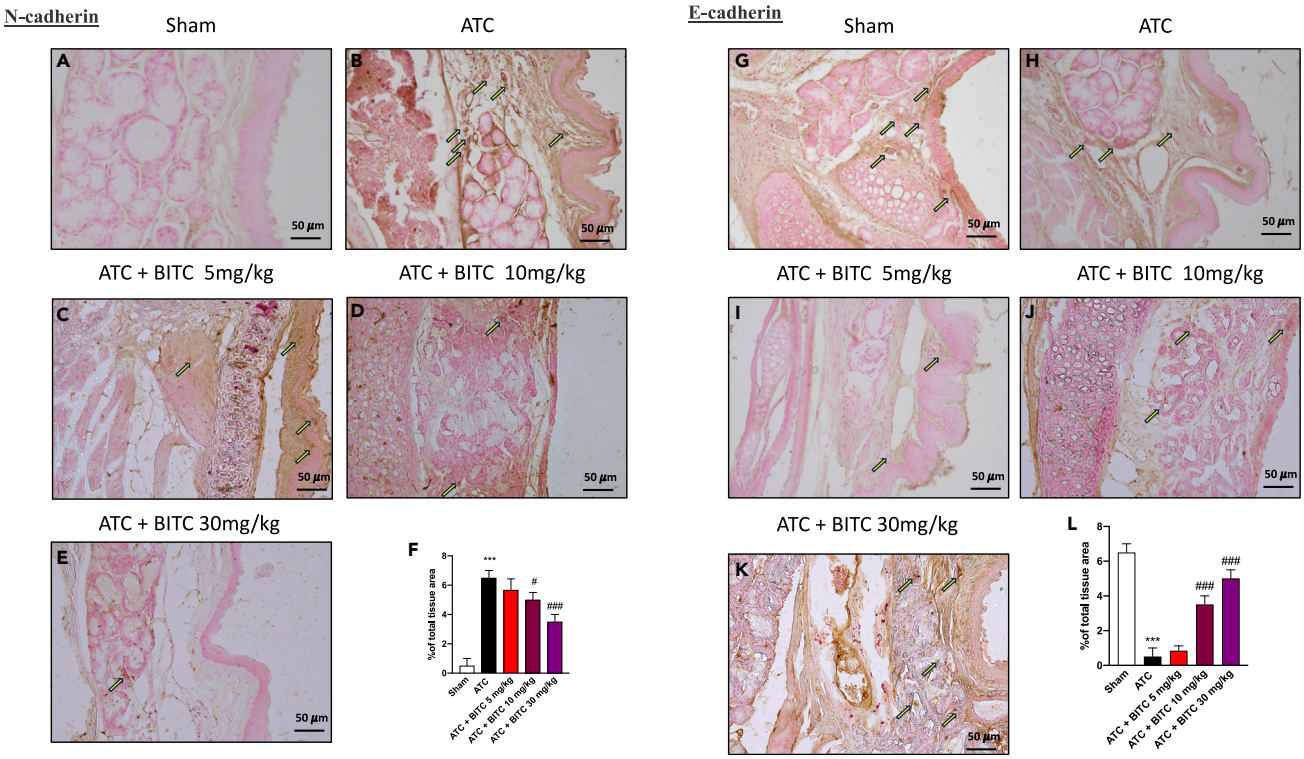

Figure 7. Effect of BITC on EMT markers in an orthotopic model of ATC

The immunohistochemical assay revealed a significant increase of N-cadherin expression in the ATC group (B) compared to Sham mice (A); this expression was reduced following treatment with BITC at doses of 10 mg/kg (D) and 30 mg/kg (E) compared to ATC group (B). BITC at the dose of 5 mg/kg did not show significant effect (C, see score panel F). At the same time the staining revelated a significant reduction of E-cadherin expression in the ATC group (H), compared to Sham mice (G); 10 mg/kg (J) and 30 mg/kg (K) BITC treatments caused an important increase of E-cadherin expression compared to ATC group (H). BITC at the dose of 5 mg/kg did not show significant effect (I, see score panel L). The data are representative of at least three independent experiments. The sections were observed and photographed at 20× magnification. Values are means ± SEM. One-way ANOVA test followed by Bonferroni post hoc test for multiple comparisons. ***$p < 0.001$ vs. Sham; #$p < 0.05$ vs. ATC; ##$p < 0.01$ vs. ATC; ###$p < 0.001$ vs. ATC.

antiapoptotic factors such as BCL-2. The induction of the apoptotic process was confirmed by the DNA fragmentation assay and is mediated by the activation of caspase-3. These findings are in line with some works that considers the disruption of mitochondrial integrity caused by BITC to be the main mechanism of induction of apoptosis related to the upregulation of the expression of the pro-apoptotic proteins Bax, Bad and the downregulation of the anti-apoptotic proteins Bcl-2 and Bcl-xL. This mechanism of regulation of mitochondrial dynamics through modulation of proteins involved in mitochondrial fusion-fission has been found in estrogen-responsive (MCF-7) and estrogen-independent (MDA-MB-231) human breast cancer cells.[43] Some *in vivo* studies have also demonstrated the tendency to BITC-mediated downregulation of proteins involved in the regulation of mitochondrial dynamics in mammary tumors of MMTV-neu mice and in addition oral administration of BITC increased the expression of the pro-apoptotic proteins caspase-3 and Bax in nude mice affected by GBM 8401 tumor.[44] Tumor development is often linked to the overexpression of cell cycle proteins, while the prospect of inhibiting these proteins and enhancing gene expression to control cell proliferation is a promising strategy in preventing cancer progression. Numerous studies have explored the ability of BITC to hinder cell cycle proteins. BITC has been shown to inhibit the proliferation of mouse TRAMP-C2 prostate cancer cells by inducing G1 cell-cycle arrest through downregulation of CDK2, CDK4, cyclin A, and cyclin D1 proteins.[20] BITC also induces substantial G2/M arrest and reduces G1 and S phase populations in human multiple myeloma MM U266 cells[45] and in human pancreatic cancer cells Capan-2 by activating Chk2, Cdc25C, Cdc-2, the cyclin-dependent kinase inhibitor p21Waf1/Cip1, and downregulating cyclin B1 proteins.[46] Our findings revealed the ability of BITC to induce cell-cycle arrest through the downregulation of CDK2 and cyclin A, confirming the role in blocking the transition from G1 phase to S phase, but also G2 phase. The EMT is a distinctive process of metastatic disease, characterized by the loss of cell-to-cell adhesion capabilities and the consequent transition to a mesenchymal phenotype, which results in increased cell plasticity and motility, as well as resistance to apoptosis.[33] The loss of E-cadherin leads to activation of the Wnt/β-catenin pathway and subsequent transcription of genes that promote proliferation and migration. Our results showed that BITC treatments were able to reduce the migration and invasiveness both *in vitro* and *in vivo* and to promote the expression of E-cadherin and the loss of genes typically expressed in mesenchymal cells, like N-cadherin and S100. Moreover, BITC has demonstrated significant efficacy in reducing distant pulmonary metastases. These data are consistent with the evidences demonstrating the ability of BITC to inhibit EMT by upregulating adherent junction proteins such as E-cadherin and

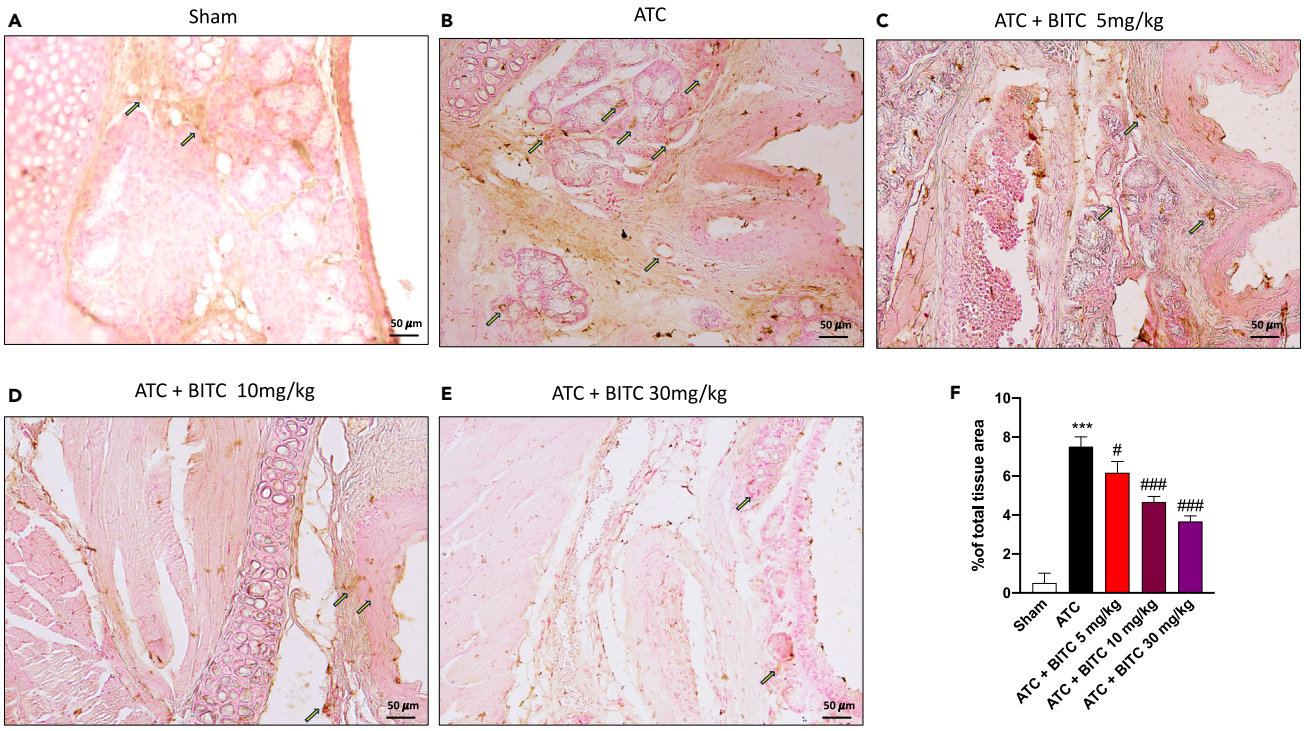

Figure 8. Effect of BITC on S100 expression in an orthotopic model of ATC

(A, B, D, and E) The immunohistochemical assay revealed a significant increase of S100 expression in the ATC group (B) compared to Sham mice (A); this expression was reduced following treatment with BITC at doses of 5 mg/kg (C),10 mg/kg (D) and 30 mg/kg (E) compared to ATC group (B) (see score F). The data are representative of at least three independent experiments. The sections were observed and photographed at 20× magnification. Values are means ± SEM. One-way ANOVA test followed by Bonferroni post hoc test for multiple comparisons. ***$p < 0.001$ vs. Sham; #$p < 0.05$ vs. ATC.

occludin, along with the downregulation of mesenchymal markers such as vimentin and fibronectin in both highly metastatic HN12 head and neck cancer cells, both MDA-MB-231 and MCF-7 breast cancer cells.[15,47]

Growing evidence suggests that the immune response may influence tumorigenesis and thyroid cancer progression.[23,48] Networks of cytokines and chemokines present in the tumor microenvironment appear to be involved in the development of the immune response may influence the progression of thyroid cancer. IL-17 is a cytokine produced by a subset of lymphocytes known as Th17 cells and shows an important function in inducing the production of high concentrations of IL-1β, TNF-α, TGF-β, chemokine, and matrix metalloproteinase mediators that are widely present in the tumor microenvironment.[49] L-17R is ubiquitously expressed, therefore, most cells are potential targets of IL-17 action. Mounting evidence shows that members of the IL-17 family play an active role not only in inflammatory and autoimmune diseases, but also in cancer. Since IL-17 is involved in the pathogenesis of chronic inflammatory responses and is known to induce the production of high concentrations of IL-1β, TNF-α, TGF-β, CC chemokine ligand (CCL)2, and matrix metalloproteinase mediators that are widely found in the tumor microenvironment, this cytokine presents a potential target that requires investigation. Tumor necrosis factor receptor (TNFR)-associated factors 6 (TRAF6) is part of the heterotrimeric complex required for IL-17 signaling and gene expression[50] and is implicated in the downregulation of the NF-κB pathway while promoting the P38 MAPK pathway. In addition, several members of the cytokine family, including IL-12, can regulate IL-17 responses. Some studies have shown that several thyroid cancer cell lines, including poorly differentiated and anaplastic TCs are positive for IL-17, suggesting a significant association between the Th17 profile and thyroid malignancies and providing the rationale for our investigations.[50–52] In this work we demonstrated that BITC treatment was able to reduce IL-17, IL-12p70 levels, and TRAF6 expression and to increase pP38, suggesting a key role also in the modification of the immune response and in the reduction of inflammatory cytokine levels in the tumor microenvironment.

Conclusions

Based on the promising antitumor effects shown by BITC in different types of solid tumors, in this article we hypothesized for the first time that BITC might be able to reduce the progression of ATC, representing a viable therapeutic alternative for the treatment of this aggressive form of tumor. The results obtained both *in vitro* and *in vivo* support this hypothesis and suggest that BITC treatment has the potential to influence various cellular processes such as autophagy, apoptosis, cell cycle, EMT, and inflammation in thyroid cancer. The biological activity of the antitumor property of BITC was further supported by the principal component analysis (PCA) analysis conducted in order to correlate all the parameters taken into consideration. This indicates that BITC may have a role in affecting the development of thyroid cancer by regulating pathways related to autophagy and apoptosis. Although further studies are required to confirm these initial findings especially in human

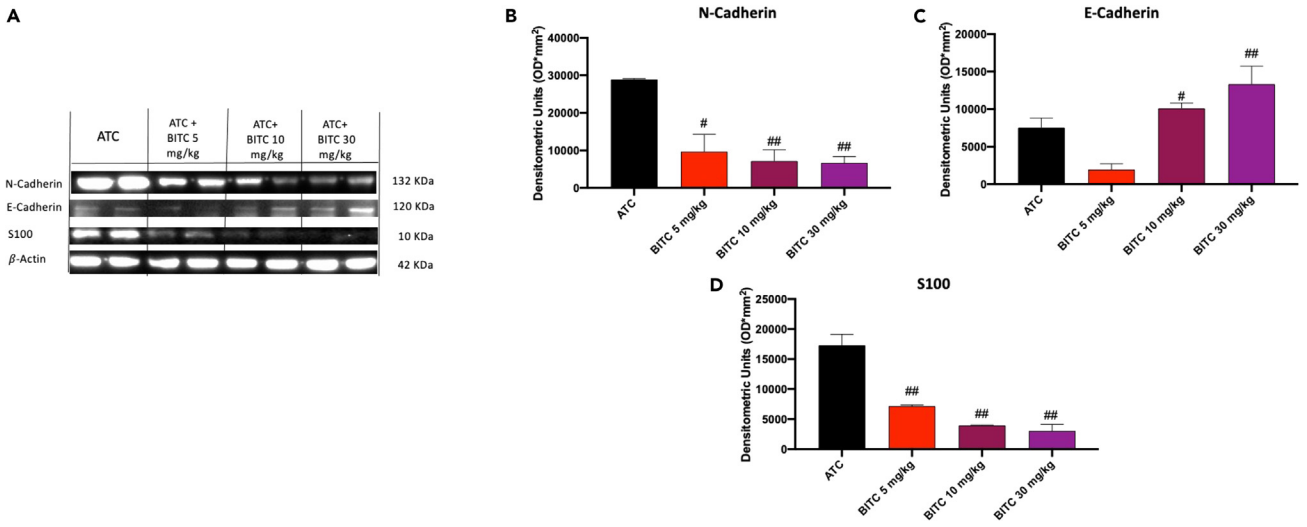

Figure 9. Effect of BITC on EMT markers expression in an orthotopic model of ATC

(A) The blots revealed a significant modulation of EMT markers expression following BITC treatment.

(B–D) BITC at the doses of 5 mg/kg, 10 mg/kg and 30 mg/kg was able to significantly reduce the expression of N-cadherin (B) and S100 (D) #$p < 0.05$, ##$p < 0.01$ vs. ATC; at the same time 10 mg/kg and 30 mg/kg BITC treatment significantly increased the expression of E-cadherin (C) compared to ATC group; #$p < 0.05$ vs. ATC; ##$p < 0.01$ vs. ATC. Values are means ± SEM. We used one-way ANOVA test followed by Bonferroni post hoc test for multiple comparisons.

clinical trials, to better understand its safety and effectiveness in cancer prevention and treatment, BITC could be explored as a potential therapeutic approach for managing thyroid cancer. We believe that the article may represent a novelty as for the first time the effects of BITC on anaplastic thyroid cancer have been investigated.

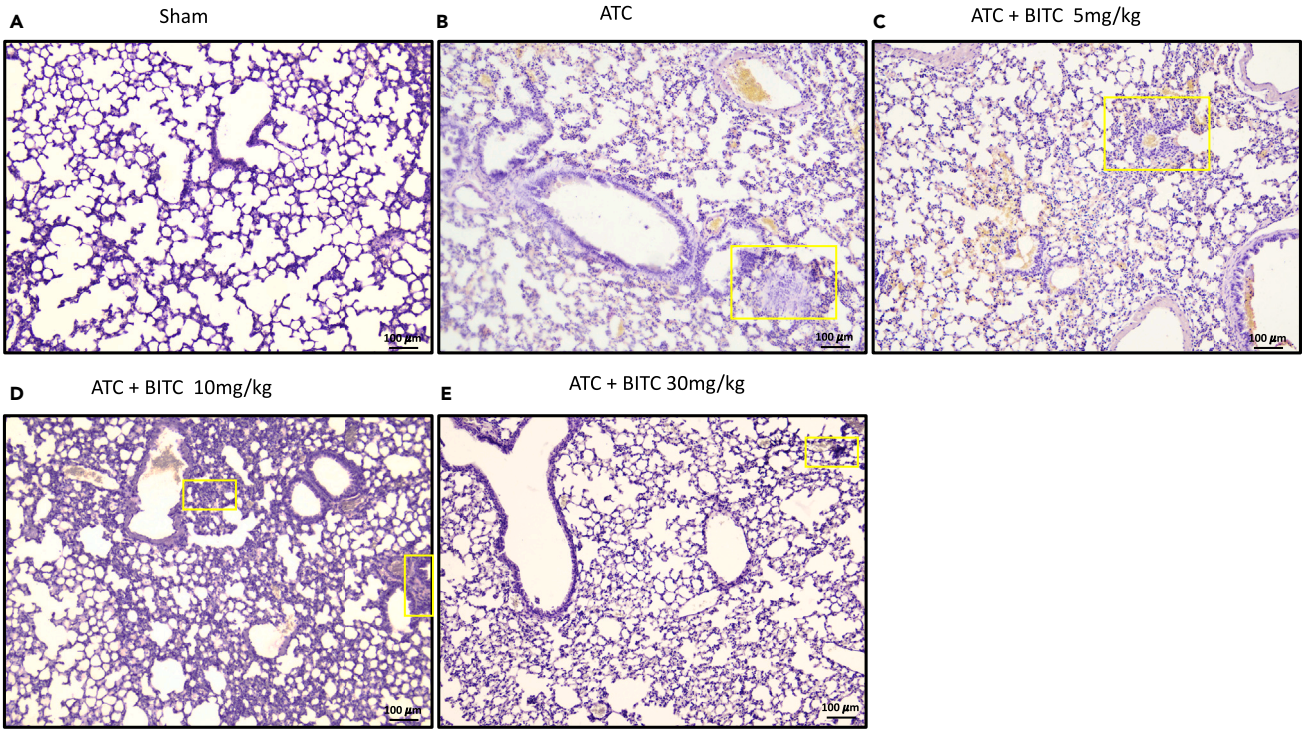

Figure 10. Effect of BITC on lung metastases

(A, D, and E) Hematoxylin and Eosin staining revelated lung metastasis in the ATC group (B), compared to sham group (A). BITC treatments at the concentrations of 10 mg/kg (D) and 30 mg/kg (E) were able to reduce distant lung metastases compared to ATC group (B). BITC treatment at the dose of 5 mg/kg did not demonstrate a significant effect (C).

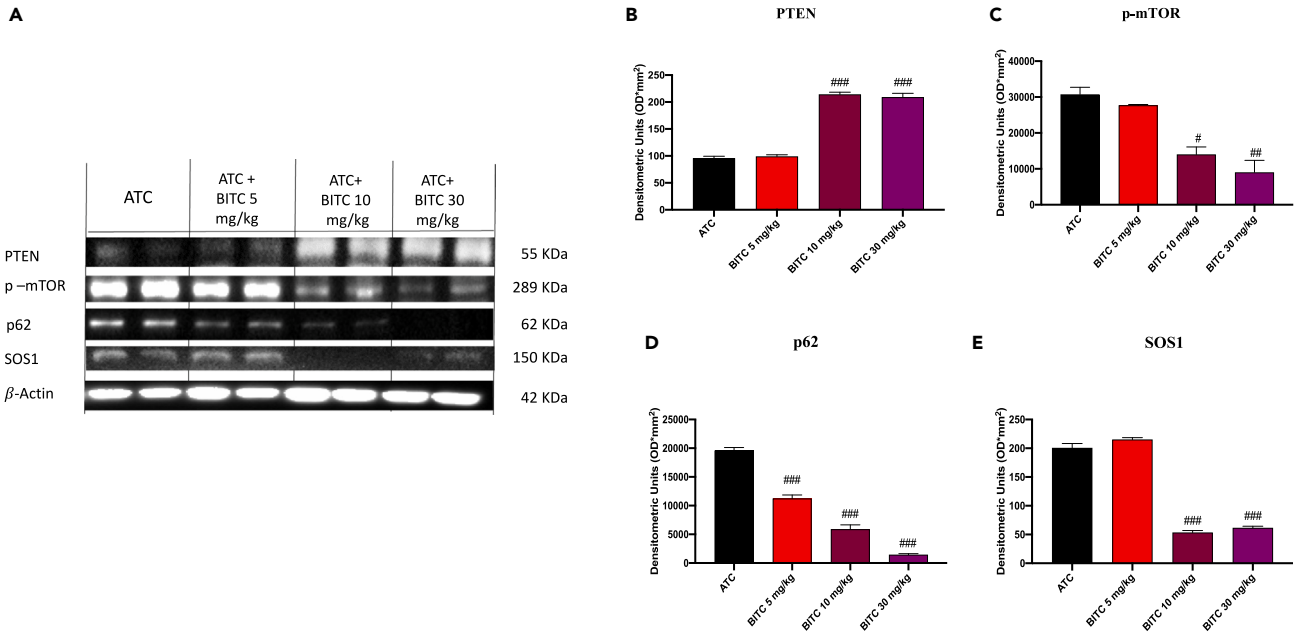

Figure 11. Effect of BITC on autophagy markers expression in an orthotopic model of ATC

(A) The blots revealed a significant modulation of autophagy markers expression following BITC treatment.

(B–E) BITC at the doses of 10 mg/kg and 30 mg/kg was able to significantly increase the expression of PTEN (B), and reduce *p*-mTOR (C), p62 (D) and SOS-1(E) proteins; #$p < 0.05$ vs. ATC; ##$p < 0.01$ vs. ATC; ###$p < 0.001$ vs. ATC. Values are means ± SEM. We used one-way ANOVA test followed by Bonferroni post hoc test for multiple comparisons.

Limitations of the study

Despite the promising results obtained, these are still preliminary studies, carried out on a pre-existing model that involves short-term treatment. It would therefore be appropriate to evaluate the effects of prolonged treatment and the resulting adverse events through a chronic toxicity study. Although the anti-tumor properties of BITC have been studied in a large variety of tumor types, this represents innovative work as for the first time these studies have been applied to ATC, a very aggressive tumor with a poor prognosis and lacking valid therapeutic approaches.

RESOURCE AVAILABILITY

Lead contact

Further information and requests for resources and reagents should be directed to and will be fulfilled by the lead contact, Emanuela Esposito (emanuela.esposito@unime.it).

Materials availability

This study did not generate new unique reagents.

Data and code availability

All data reported in this paper will be shared by the lead contact upon request.

This paper does not report original code.

Any additional information required to reanalyze the data reported in this paper is available from the lead contact upon request.

ACKNOWLEDGMENTS

Not applicable.

AUTHOR CONTRIBUTIONS

Conceptualization, E.E. and I.P.; methodology, R.B. and D.M.; formal analysis, A.F. and M.L.; investigation, R.B. and G.C.; resources A.P.C., L.C., and D.S.; data curation, G.C.; writing – original draft preparation, R.B.; writing – review and editing G.C.; supervision, S.F., I.P., and E.E.; all authors have read and agreed to the published version of the manuscript.

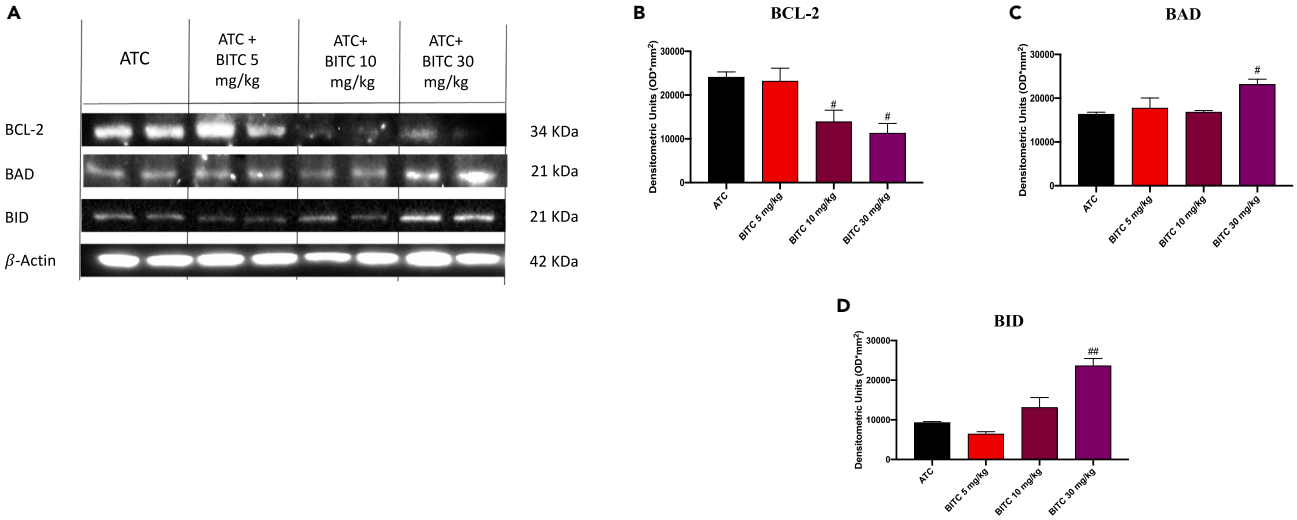

Figure 12. Effect of BITC on apoptosis markers expression in an orthotopic model of ATC

(A) The blots revealed a significant modulation of apoptosis markers expression following BITC treatment.

(B–D) BITC at the doses of 10 mg/kg and 30 mg/kg was able to significantly reduce the expression of anti-apoptotic protein BCL-2 (B) #$p < 0.05$ vs. ATC; at the same time 30 mg/kg BITC treatment increased the expression of pro-apoptotic BAD (C), and BID (D) markers compared to ATC group; #$p < 0.05$ vs. ATC; ##$p < 0.01$ vs. ATC. Values are means ± SEM. We used one-way ANOVA test followed by Bonferroni post hoc test for multiple comparisons.

DECLARATION OF INTERESTS

The authors declare no competing interests.

STAR★METHODS

Detailed methods are provided in the online version of this paper and include the following:

- KEY RESOURCES TABLE
- EXPERIMENTAL MODEL AND STUDY PARTICIPANT DETAILS
  - Cell cultures
  - Animals
- METHOD DETAILS
  - *In vitro* studies
  - In *vivo studies*
- QUANTIFICATION AND STATISTICAL ANALYSIS
  - Statistical analysis
  - Principal component analysis (PCA)

SUPPLEMENTAL INFORMATION

Supplemental information can be found online at https://doi.org/10.1016/j.isci.2024.110796.

Received: February 16, 2024
Revised: May 9, 2024
Accepted: August 20, 2024
Published: August 23, 2024

REFERENCES

1. Baloch, Z.W., Asa, S.L., Barletta, J.A., Ghossein, R.A., Juhlin, C.C., Jung, C.K., LiVolsi, V.A., Papotti, M.G., Sobrinho-Simões, M., Tallini, G., and Mete, O. (2022). Overview of the 2022 WHO Classification of Thyroid Neoplasms. Endocr. Pathol. *33*, 27–63. https://doi.org/10.1007/s12022-022-09707-3.

2. Asa, S.L. (2019). The Current Histologic Classification of Thyroid Cancer. Endocrinol. Metab. Clin. North Am. *48*, 1–22. https://doi.org/10.1016/j.ecl.2018.10.001.

3. Abe, I., and Lam, A.K.Y. (2021). Anaplastic thyroid carcinoma: Updates on WHO classification, clinicopathological features and staging. Histol. Histopathol. *36*, 239–248. https://doi.org/10.14670/HH-18-277.

4. US Preventive Services Task Force, Bibbins-Domingo, K., Grossman, D.C., Curry, S.J., Barry, M.J., Davidson, K.W., Doubeni, C.A., Epling, J.W., Jr., Kemper, A.R., Krist, A.H., et al. (2017). Screening for Thyroid Cancer: US Preventive Services Task Force Recommendation Statement. JAMA *317*, 1882–1887. https://doi.org/10.1001/jama.2017.4011.

5. Haddad, R.I., Bischoff, L., Ball, D., Bernet, V., Blomain, E., Busaidy, N.L., Campbell, M., Dickson, P., Duh, Q.Y., Ehya, H., et al. (2022). Thyroid Carcinoma, Version 2.2022, NCCN Clinical Practice Guidelines in Oncology.

J. Natl. Compr. Canc. Netw. *20*, 925–951. https://doi.org/10.6004/jnccn.2022.0040.
6. DeGroot, L.J., and Zhang, R. (2001). Clinical review 131: Gene therapy for thyroid cancer: where do we stand? J. Clin. Endocrinol. Metab. *86*, 2923–2928. https://doi.org/10.1210/jcem.86.7.7653.
7. Zhang, Y., Xing, Z., Liu, T., Tang, M., Mi, L., Zhu, J., Wu, W., and Wei, T. (2022). Targeted therapy and drug resistance in thyroid cancer. Eur. J. Med. Chem. *238*, 114500. https://doi.org/10.1016/j.ejmech.2022.114500.
8. Laha, D., Nilubol, N., and Boufraqech, M. (2020). New Therapies for Advanced Thyroid Cancer. Front. Endocrinol. *11*, 82. https://doi.org/10.3389/fendo.2020.00082.
9. Kim, E.J., Eom, S.J., Hong, J.E., Lee, J.Y., Choi, M.S., and Park, J.H.Y. (2012). Benzyl isothiocyanate inhibits basal and hepatocyte growth factor-stimulated migration of breast cancer cells. Mol. Cell. Biochem. *359*, 431–440. https://doi.org/10.1007/s11010-011-1039-3.
10. Po, W.W., Choi, W.S., Khing, T.M., Lee, J.Y., Lee, J.H., Bang, J.S., Min, Y.S., Jeong, J.H., and Sohn, U.D. (2022). Benzyl Isothiocyanate-Induced Cytotoxicity via the Inhibition of Autophagy and Lysosomal Function in AGS Cells. Biomol. Ther. *30*, 348–359. https://doi.org/10.4062/biomolther.2022.019.
11. Lin, J.F., Tsai, T.F., Yang, S.C., Lin, Y.C., Chen, H.E., Chou, K.Y., and Hwang, T.I.S. (2017). Benzyl isothiocyanate induces reactive oxygen species-initiated autophagy and apoptosis in human prostate cancer cells. Oncotarget *8*, 20220–20234. https://doi.org/10.18632/oncotarget.15643.
12. Brüsewitz, G., Cameron, B.D., Chasseaud, L.F., Gorler, K., Hawkins, D.R., Koch, H., and Mennicke, W.H. (1977). The metabolism of benzyl isothiocyanate and its cysteine conjugate. Biochem. J. *162*, 99–107. https://doi.org/10.1042/bj1620099.
13. Dufour, V., Alazzam, B., Ermel, G., Thepaut, M., Rossero, A., Tresse, O., and Baysse, C. (2012). Antimicrobial activities of isothiocyanates against Campylobacter jejuni isolates. Front. Cell. Infect. Microbiol. *2*, 53. https://doi.org/10.3389/fcimb.2012.00053.
14. Platz, S., Kühn, C., Schiess, S., Schreiner, M., Kemper, M., Pivovarova, O., Pfeiffer, A.F.H., and Rohn, S. (2016). Bioavailability and metabolism of benzyl glucosinolate in humans consuming Indian cress (Tropaeolum majus L.). Mol. Nutr. Food Res. *60*, 652–660. https://doi.org/10.1002/mnfr.201500633.
15. Sehrawat, A., and Singh, S.V. (2011). Benzyl isothiocyanate inhibits epithelial-mesenchymal transition in cultured and xenografted human breast cancer cells. Cancer Prev. Res. *4*, 1107–1117. https://doi.org/10.1158/1940-6207.CAPR-10-0306.
16. Lin, J.F., Tsai, T.F., Lin, Y.C., Chen, H.E., Chou, K.Y., and Hwang, T.I.S. (2019). Benzyl isothiocyanate suppresses IGF1R, FGFR3 and mTOR expression by upregulation of miR-99a-5p in human bladder cancer cells. Int. J. Oncol. *54*, 2106–2116. https://doi.org/10.3892/ijo.2019.4763.
17. Zhang, Q.C., Pan, Z.H., Liu, B.N., Meng, Z.W., Wu, X., Zhou, Q.H., and Xu, K. (2017). Benzyl isothiocyanate induces protective autophagy in human lung cancer cells through an endoplasmic reticulum stress-mediated mechanism. Acta Pharmacol. Sin. *38*, 539–550. https://doi.org/10.1038/aps.2016.146.
18. Liu, X., Abe-Kanoh, N., Liu, Y., Zhu, B., Munemasa, S., Nakamura, T., Murata, Y., and Nakamura, Y. (2017). Inhibition of phosphatidylinositide 3-kinase impairs the benzyl isothiocyanate-induced accumulation of autophagic molecules and Nrf2 in human colon cancer cells. Biosci. Biotechnol. Biochem. *81*, 2212–2215. https://doi.org/10.1080/09168451.2017.1374830.
19. Xie, B., Nagalingam, A., Kuppusamy, P., Muniraj, N., Langford, P., Győrffy, B., Saxena, N.K., and Sharma, D. (2017). Benzyl Isothiocyanate potentiates p53 signaling and antitumor effects against breast cancer through activation of p53-LKB1 and p73-LKB1 axes. Sci. Rep. *7*, 40070. https://doi.org/10.1038/srep40070.
20. Cho, H.J., Lim, D.Y., Kwon, G.T., Kim, J.H., Huang, Z., Song, H., Oh, Y.S., Kang, Y.H., Lee, K.W., Dong, Z., and Park, J.H.Y. (2016). Benzyl Isothiocyanate Inhibits Prostate Cancer Development in the Transgenic Adenocarcinoma Mouse Prostate (TRAMP) Model, Which Is Associated with the Induction of Cell Cycle G1 Arrest. Int. J. Mol. Sci. *17*, 264. https://doi.org/10.3390/ijms17020264.
21. Lai, K.C., Huang, A.C., Hsu, S.C., Kuo, C.L., Yang, J.S., Wu, S.H., and Chung, J.G. (2010). Benzyl isothiocyanate (BITC) inhibits migration and invasion of human colon cancer HT29 cells by inhibiting matrix metalloproteinase-2/-9 and urokinase plasminogen (uPA) through PKC and MAPK signaling pathway. J. Agric. Food Chem. *58*, 2935–2942. https://doi.org/10.1021/jf9036694.
22. Lin, J.F., Tsai, T.F., Liao, P.C., Lin, Y.H., Lin, Y.C., Chen, H.E., Chou, K.Y., and Hwang, T.I.S. (2013). Benzyl isothiocyanate induces protective autophagy in human prostate cancer cells via inhibition of mTOR signaling. Carcinogenesis *34*, 406–414. https://doi.org/10.1093/carcin/bgs359.
23. Guarino, V., Castellone, M.D., Avilla, E., and Melillo, R.M. (2010). Thyroid cancer and inflammation. Mol. Cell. Endocrinol. *321*, 94–102. https://doi.org/10.1016/j.mce.2009.10.003.
24. Nucera, C., Nehs, M.A., Mekel, M., Zhang, X., Hodin, R., Lawler, J., Nose, V., and Parangi, S. (2009). A novel orthotopic mouse model of human anaplastic thyroid carcinoma. Thyroid *19*, 1077–1084. https://doi.org/10.1089/thy.2009.0055.
25. Shakib, H., Rajabi, S., Dehghan, M.H., Mashayekhi, F.J., Safari-Alighiarloo, N., and Hedayati, M. (2019). Epithelial-to-mesenchymal transition in thyroid cancer: a comprehensive review. Endocrine *66*, 435–455. https://doi.org/10.1007/s12020-019-02030-8.
26. Zou, M., Al-Baradie, R.S., Al-Hindi, H., Farid, N.R., and Shi, Y. (2005). S100A4 (Mts1) gene overexpression is associated with invasion and metastasis of papillary thyroid carcinoma. Br. J. Cancer *93*, 1277–1284. https://doi.org/10.1038/sj.bjc.6602856.
27. Zou, M., Famulski, K.S., Parhar, R.S., Baitei, E., Al-Mohanna, F.A., Farid, N.R., and Shi, Y. (2004). Microarray analysis of metastasis-associated gene expression profiling in a murine model of thyroid carcinoma pulmonary metastasis: identification of S100A4 (Mts1) gene overexpression as a poor prognostic marker for thyroid carcinoma. J. Clin. Endocrinol. Metab. *89*, 6146–6154. https://doi.org/10.1210/jc.2004-0418.
28. Shi, Y., Zou, M., Collison, K., Baitei, E.Y., Al-Makhalafi, Z., Farid, N.R., and Al-Mohanna, F.A. (2006). Ribonucleic acid interference targeting S100A4 (Mts1) suppresses tumor growth and metastasis of anaplastic thyroid carcinoma in a mouse model. J. Clin. Endocrinol. Metab. *91*, 2373–2379. https://doi.org/10.1210/jc.2006-0155.
29. Salama, I., Malone, P.S., Mihaimeed, F., and Jones, J.L. (2008). A review of the S100 proteins in cancer. Eur. J. Surg. Oncol. *34*, 357–364. https://doi.org/10.1016/j.ejso.2007.04.009.
30. Besic, N., and Gazic, B. (2013). Sites of metastases of anaplastic thyroid carcinoma: autopsy findings in 45 cases from a single institution. Thyroid *23*, 709–713. https://doi.org/10.1089/thy.2012.0252.
31. Yang, J., and Barletta, J.A. (2020). Anaplastic thyroid carcinoma. Semin. Diagn. Pathol. *37*, 248–256. https://doi.org/10.1053/j.semdp.2020.06.005.
32. Ferrari, S.M., Elia, G., Ragusa, F., Ruffilli, I., La Motta, C., Paparo, S.R., Patrizio, A., Vita, R., Benvenga, S., Materazzi, G., et al. (2020). Novel treatments for anaplastic thyroid carcinoma. Gland Surg. *9*, S28–S42. https://doi.org/10.21037/gs.2019.10.18.
33. Holm, T.M., Yeo, S., Turner, K.M., and Guan, J.L. (2022). Targeting Autophagy in Thyroid Cancer: EMT, Apoptosis, and Cancer Stem Cells. Front. Cell Dev. Biol. *10*, 821855. https://doi.org/10.3389/fcell.2022.821855.
34. Netea-Maier, R.T., Klück, V., Plantinga, T.S., and Smit, J.W.A. (2015). Autophagy in thyroid cancer: present knowledge and future perspectives. Front. Endocrinol. *6*, 22. https://doi.org/10.3389/fendo.2015.00022.
35. Abe, I., and Lam, A.K.Y. (2021). Anaplastic Thyroid Carcinoma: Current Issues in Genomics and Therapeutics. Curr. Oncol. Rep. *23*, 31. https://doi.org/10.1007/s11912-021-01019-9.
36. Milosevic, Z., Pesic, M., Stankovic, T., Dinic, J., Milovanovic, Z., Stojsic, J., Dzodic, R., Tanic, N., and Bankovic, J. (2014). Targeting RAS-MAPK-ERK and PI3K-AKT-mTOR signal transduction pathways to chemosensitize anaplastic thyroid carcinoma. Transl. Res. *164*, 411–423. https://doi.org/10.1016/j.trsl.2014.06.005.
37. Wong, K., Di Cristofano, F., Ranieri, M., De Martino, D., and Di Cristofano, A. (2019). PI3K/mTOR inhibition potentiates and extends palbociclib activity in anaplastic thyroid cancer. Endocr. Relat. Cancer *26*, 425–436. https://doi.org/10.1530/ERC-19-0011.
38. Hanly, E.K., Bednarczyk, R.B., Tuli, N.Y., Moscatello, A.L., Halicka, H.D., Li, J., Geliebter, J., Darzynkiewicz, Z., and Tiwari, R.K. (2015). mTOR inhibitors sensitize thyroid cancer cells to cytotoxic effect of vemurafenib. Oncotarget *6*, 39702–39713. https://doi.org/10.18632/oncotarget.4052.
39. Duran, A., Amanchy, R., Linares, J.F., Joshi, J., Abu-Baker, S., Porollo, A., Hansen, M., Moscat, J., and Diaz-Meco, M.T. (2011). p62 is a key regulator of nutrient sensing in the mTORC1 pathway. Mol. Cell *44*, 134–146. https://doi.org/10.1016/j.molcel.2011.06.038.
40. Mendoza, M.C., Er, E.E., and Blenis, J. (2011). The Ras-ERK and PI3K-mTOR pathways: cross-talk and compensation. Trends Biochem. Sci. *36*, 320–328. https://doi.org/10.1016/j.tibs.2011.03.006.
41. Chen, Y., and Gibson, S.B. (2021). Three dimensions of autophagy in regulating tumor growth: cell survival/death, cell proliferation, and tumor dormancy. Biochim. Biophys.

Acta, Mol. Basis Dis. *1867*, 166265. https://doi.org/10.1016/j.bbadis.2021.166265.
42. Xiao, D., Bommareddy, A., Kim, S.H., Sehrawat, A., Hahm, E.R., and Singh, S.V. (2012). Benzyl isothiocyanate causes FoxO1-mediated autophagic death in human breast cancer cells. PLoS One *7*, e32597. https://doi.org/10.1371/journal.pone.0032597.
43. Sehrawat, A., Croix, C.S., Baty, C.J., Watkins, S., Tailor, D., Singh, R.P., and Singh, S.V. (2016). Inhibition of mitochondrial fusion is an early and critical event in breast cancer cell apoptosis by dietary chemopreventative benzyl isothiocyanate. Mitochondrion *30*, 67–77. https://doi.org/10.1016/j.mito.2016.06.006.
44. Ma, Y.S., Lin, J.J., Lin, C.C., Lien, J.C., Peng, S.F., Fan, M.J., Hsu, F.T., and Chung, J.G. (2018). Benzyl isothiocyanate inhibits human brain glioblastoma multiforme GBM 8401 cell xenograft tumor in nude mice *in vivo*. Environ. Toxicol. *33*, 1097–1104. https://doi.org/10.1002/tox.22581.
45. Mi, L., Gan, N., and Chung, F.L. (2011). Isothiocyanates inhibit proteasome activity and proliferation of multiple myeloma cells. Carcinogenesis *32*, 216–223. https://doi.org/10.1093/carcin/bgq242.
46. Zhang, R., Loganathan, S., Humphreys, I., and Srivastava, S.K. (2006). Benzyl isothiocyanate-induced DNA damage causes G2/M cell cycle arrest and apoptosis in human pancreatic cancer cells. J. Nutr. *136*, 2728–2734. https://doi.org/10.1093/jn/136.11.2728.
47. Sehrawat, A., Kim, S.H., Vogt, A., and Singh, S.V. (2013). Suppression of FOXQ1 in benzyl isothiocyanate-mediated inhibition of epithelial-mesenchymal transition in human breast cancer cells. Carcinogenesis *34*, 864–873. https://doi.org/10.1093/carcin/bgs397.
48. Ferrari, S.M., Fallahi, P., Galdiero, M.R., Ruffilli, I., Elia, G., Ragusa, F., Paparo, S.R., Patrizio, A., Mazzi, V., Varricchi, G., et al. (2019). Immune and Inflammatory Cells in Thyroid Cancer Microenvironment. Int. J. Mol. Sci. *20*, 4413. https://doi.org/10.3390/ijms20184413.
49. Carvalho, D.F.G., Zanetti, B.R., Miranda, L., Hassumi-Fukasawa, M.K., Miranda-Camargo, F., Crispim, J.C.O., and Soares, E.G. (2017). High IL-17 expression is associated with an unfavorable prognosis in thyroid cancer. Oncol. Lett. *13*, 1925–1931. https://doi.org/10.3892/ol.2017.5638.
50. Rong, Z., Wang, A., Li, Z., Ren, Y., Cheng, L., Li, Y., Wang, Y., Ren, F., Zhang, X., Hu, J., and Chang, Z. (2009). IL-17RD (Sef or IL-17RLM) interacts with IL-17 receptor and mediates IL-17 signaling. Cell Res. *19*, 208–215. https://doi.org/10.1038/cr.2008.320.
51. Bohnsack, J.F., Chang, J.K., and Hill, H.R. (1993). Restricted ability of group B streptococcal C5a-ase to inactivate C5a prepared from different animal species. Infect. Immun. *61*, 1421–1426. https://doi.org/10.1128/iai.61.4.1421-1426.1993.
52. Kolls, J.K., and Lindén, A. (2004). Interleukin-17 family members and inflammation. Immunity *21*, 467–476. https://doi.org/10.1016/j.immuni.2004.08.018.
53. Kim, S., Prichard, C.N., Younes, M.N., Yazici, Y.D., Jasser, S.A., Bekele, B.N., and Myers, J.N. (2006). Cetuximab and irinotecan interact synergistically to inhibit the growth of orthotopic anaplastic thyroid carcinoma xenografts in nude mice. Clin. Cancer Res. *12*, 600–607.
54. Banchi, M., Orlandi, P., Gentile, D., Alì, G., Fini, E., Fontanini, G., Francia, G., and Bocci, G. (2020). Synergistic activity of linifanib and irinotecan increases the survival of mice bearing orthotopically implanted human anaplastic thyroid cancer. Am. J. Cancer Res. *10*, 2120–2127.
55. Kim, S., Yazici, Y.D., Calzada, G., Wang, Z.-Y., Younes, M.N., Jasser, S.A., El-Naggar, A.K., and Myers, J.N. (2007). Sorafenib inhibits the angiogenesis and growth of orthotopic anaplastic thyroid carcinoma xenografts in nude mice. Mol. Cancer Ther. *6*, 1785–1792.
56. Prichard, C.N., Kim, S., Yazici, Y.D., Doan, D.D., Jasser, S.A., Mandal, M., and Myers, J.N. (2007). Concurrent cetuximab and bevacizumab therapy in a murine orthotopic model of anaplastic thyroid carcinoma. Laryngoscope *117*, 674–679.
57. Kim, S., Yazici, Y.D., Barber, S.E., Jasser, S.A., Mandal, M., Bekele, B.N., and Myers, J.N. (2006). Growth inhibition of orthotopic anaplastic thyroid carcinoma xenografts in nude mice by PTK787/ZK222584 and CPT-11. Head Neck *28*, 389–399.
58. Gule, M.K., Chen, Y., Sano, D., Frederick, M.J., Zhou, G., Zhao, M., Milas, Z.L., Galer, C.E., Henderson, Y.C., Jasser, S.A., et al. (2011). Targeted therapy of VEGFR2 and EGFR significantly inhibits growth of anaplastic thyroid cancer in an orthotopic murine model. Clin. Cancer Res. *17*, 2281–2291.
59. Scuderi, S.A., Casili, G., Filippone, A., Lanza, M., Basilotta, R., Giuffrida, R., Munaò, S., Colarossi, L., Capra, A.P., Esposito, E., and Paterniti, I. (2021). Beneficial effect of KYP-2047, a propyl-oligopeptidase inhibitor, on oral squamous cell carcinoma. Oncotarget *12*, 2459–2473. https://doi.org/10.18632/oncotarget.28147.
60. Zakaria, S., Helmy, M.W., Salahuddin, A., and Omran, G. (2018). Chemopreventive and antitumor effects of benzyl isothiocynate on HCC models: A possible role of HGF/pAkt/STAT3 axis and VEGF. Biomed. Pharmacother. *108*, 65–75. https://doi.org/10.1016/j.biopha.2018.09.016.
61. Scuderi, S.A., Casili, G., Basilotta, R., Lanza, M., Filippone, A., Raciti, G., Puliafito, I., Colarossi, L., Esposito, E., and Paterniti, I. (2021). NLRP3 Inflammasome Inhibitor BAY-117082 Reduces Oral Squamous Cell Carcinoma Progression. Int. J. Mol. Sci. *22*, 11108. https://doi.org/10.3390/ijms222011108.
62. Liang, C.C., Park, A.Y., and Guan, J.L. (2007). In vitro scratch assay: a convenient and inexpensive method for analysis of cell migration *in vitro*. Nat. Protoc. *2*, 329–333. https://doi.org/10.1038/nprot.2007.30.
63. Cheng, N., Diao, H., Lin, Z., Gao, J., Zhao, Y., Zhang, W., Wang, Q., Lin, J., Zhang, D., Jin, Y., et al. (2020). Benzyl Isothiocyanate Induces Apoptosis and Inhibits Tumor Growth in Canine Mammary Carcinoma via Downregulation of the Cyclin B1/Cdk1 Pathway. Front. Vet. Sci. *7*, 580530. https://doi.org/10.3389/fvets.2020.580530.
64. Ohnishi, K., Ota, I., Yane, K., Takahashi, A., Yuki, K., Emoto, M., Hosoi, H., and Ohnishi, T. (2002). Glycerol as a chemical chaperone enhances radiation-induced apoptosis in anaplastic thyroid carcinoma cells. Mol. Cancer *1*, 4. https://doi.org/10.1186/1476-4598-1-4.
65. Sewell, W., Reeb, A., and Lin, R.Y. (2013). An orthotopic mouse model of anaplastic thyroid carcinoma. J. Vis. Exp. *74*, e50097. https://doi.org/10.3791/50097.
66. Fanfone, D., Stanicki, D., Nonclercq, D., Port, M., Vander Elst, L., Laurent, S., Muller, R.N., Saussez, S., and Burtea, C. (2020). Molecular Imaging of Galectin-1 Expression as a Biomarker of Papillary Thyroid Cancer by Using Peptide-Functionalized Imaging Probes. Biology *9*, 53. https://doi.org/10.3390/biology9030053.
67. Casili, G., Caffo, M., Campolo, M., Barresi, V., Caruso, G., Cardali, S.M., Lanza, M., Mallamace, R., Filippone, A., Conti, A., et al. (2018). TLR-4/Wnt modulation as new therapeutic strategy in the treatment of glioblastomas. Oncotarget *9*, 37564–37580. https://doi.org/10.18632/oncotarget.26500.
68. Basilotta, R., Lanza, M., Filippone, A., Casili, G., Mannino, D., De Gaetano, F., Chisari, G., Colarossi, L., Motta, G., Campolo, M., et al. (2023). Therapeutic Potential of Dimethyl Fumarate in Counteract Oral Squamous Cell Carcinoma Progression by Modulating Apoptosis, Oxidative Stress and Epithelial-Mesenchymal Transition. Int. J. Mol. Sci. *24*, 2777. https://doi.org/10.3390/ijms24032777.
69. Gonzalez, E., van Liempd, S., Conde-Vancells, J., Gutierrez-de Juan, V., Perez-Cormenzana, M., Mayo, R., Berisa, A., Alonso, C., Marquez, C.A., Barr, J., et al. (2012). Serum UPLC-MS/MS metabolic profiling in an experimental model for acute-liver injury reveals potential biomarkers for hepatotoxicity. Metabolomics *8*, 997–1011. https://doi.org/10.1007/s11306-011-0329-9.

STAR★METHODS

KEY RESOURCES TABLE

REAGENT or RESOURCE	SOURCE	IDENTIFIER
Antibodies		
Rabbit polyclonal anti-BID	Santa Cruz Biotechnology	sc-11423 lot# F2812; RRID: AB_2243383
Mouse monoclonal anti-BAX	Santa Cruz Biotechnology	sc-7480 lot# E2418; RRID: AB_626729
Mouse monoclonal anti-BCL-2	Santa Cruz Biotechnology	sc-7382 lot# I1521:RRID: AB_626736
Mouse monoclonal anti-Caspase 3	Santa Cruz Biotechnology	sc-7272 lot# K1617; RRID: AB_626803
Mouse monoclonal anti-MAP LC3	Santa Cruz Biotechnology	sc-398822 lot# F2918: RRID: AB_2877091
Rabbit antibody anti-pmTOR	Cell Signaling	S2448 lot# 21
Rabbit antibody anti-p62	Cell Signaling	5114S lot# 4
Monoclonal antibody anti-LAMP2	Invitrogen	MA1-205 lot# XI348833; RRID: AB_2662613
Phospho-p38 MAPK (Thr180/Tyr182) Antibody	Cell Signaling	9211S lot# 19
Rabbit polyclonal anti-TRAF6	Santa Cruz Biotechnology	sc-7221 lot# H0811; RRID: AB_793346
β-actin	Santa Cruz Biotechnology	sc-47778; RRID: AB_626632
Mouse monoclonal anti-GAPDH	Santa Cruz Biotechnology	sc-32233 lot# A1822; RRID: AB_627679
Mouse monoclonal anti-E-Cadherin	Santa Cruz Biotechnology	sc-8426 lot# H2720; RRID: AB_626780
Mouse monoclonal anti-N-Cadherin	Santa Cruz Biotechnology	sc-8424 lot# A1422; RRID: AB_626778
Mouse monoclonal anti-S100	Santa Cruz Biotechnology	sc-393919 lot# C1120; RRID: AB_2910203
Mouse monoclonal anti-PTEN	Santa Cruz Biotechnology	sc-7974 lot# E2023; RRID: AB_628187
Mouse monoclonal anti-SOS1	Santa Cruz Biotechnology	sc-17793 lot# H1920; RRID: AB_628269
Mouse monoclonal anti-BAD	Santa Cruz Biotechnology	sc-8044 lot# H3112; RRID: AB_626717
Chemicals, peptides, and recombinant proteins		
Benzyl isothiocyanate 98%	Sigma–Aldrich Company	252492 source STBK3105
Precision Plus protein unstained Standards	Bio-Rad	64333538
Critical commercial assays		
ELISA kit for IL-17	Cloud-Clone Corp	SEA063Mu lot# L221004357
Human IL-12p70 ELISA kit	proteintech	KE10014 lot# 40001151
Human CDK2 SimpleStep ELISA Kit	abcam	ab316258 lot# N/A
Cyclin A ELISA Kit	Biocompare	ABIN6955143 lot# N/A
REDExtract-N-Amp Tissue PCR Kit	Sigma–Aldrich Company	XNAT-100RXN lot# SLCN6053
Masson's trichrome kit	Bio-Optica	04-010802 lot# 23119
Experimental models: Cell lines		
8305C	Merk Sigma–Aldrich Company	94090183
8505C	Merk Sigma–Aldrich Company	94090184
ARO 81-1	ATCC	N/A
BHT-101	DSMZ	ACC 279 ref:14831
Nthy-0ri-3-1	Merk Sigma–Aldrich Company	90011609
Experimental models: Organisms/strains		
BALB/c nude male mice	Envigo/Inotiv	
Software and algorithms		
ImageJ	Fiji	Version 1.53
GraphPad 9.0	Prism	Version 8.4

EXPERIMENTAL MODEL AND STUDY PARTICIPANT DETAILS

Cell cultures

Human TC cell lines patient 8305C (established from undifferentiated thyroid carcinomas of a 67 year old female), 8505C (Established from undifferentiated thyroid carcinomas of a 78 year old female patient), ARO 81-1, BHT-101 (established from the lymph node metastasis of a 63-year-old woman with anaplastic thyroid carcinoma) and Nthy-0ri-3-1 were obtained from Sigma-Aldrich, St. Louis, MO, USA and ATCC American Type Culture Collection, Rockville, MD, USA. Cells were cultured in RPMI-1640 medium (Sigma-Aldrich, St. Louis, MO, USA cat. R8758) supplemented with 10% fetal bovine serum (FBS, Life Technologies, Gibco®; Carlsbad, CA, USA), 100 U/ml of penicillin and 100 μg/ml of streptomycin. All cell lines were maintained in incubators at 37°C with 5% CO2.

Cells were divided into 4 groups:

1. Control group: TC cell lines: FTC-133, K1 and 8305C;
2. BITC 30 μM group: FTC-133, K1 and 8305C cells were treated with BITC 30 μM for 24 hrs;
3. BITC 100 μM group: FTC-133, K1 and 8305C cells were treated with BITC 100 μM for 24 hrs;
4. BITC 200 μM group: FTC-133, K1 and 8305C cells were treated with BITC 200 μM for 24 hrs.

For other analysis we continued to analyze only BITC 30 μM, 100 μM and 200 μM because represented the most cytotoxic concentrations revealed by MTT assay. Moreover, since BITC showed similar effects on cell viability in all cell lines, we decided to continue to analyze the effect of BITC only on 8305C cell line because it represents one of the most frequently used cell line in the field of ATC.

Animals

For *in vivo* studies BALB/c nude male mice (25-30 g; 6-8 weeks of age) were used and purchased from Envigo (Milan, Italy). Animals were placed in a controlled environment and were fed with a standard diet and water *ad libitum* under pathogen-free conditions with a 12 h light/12 h dark. The study was approved by OPBA of Messina with the authorization number 89126.25. The use of male mice was chosen to achieve greater consistency in the results. In fact, although the prevalence of ATC is higher in females than in males, hormonal variations of female mice could affect tumor growth and response to treatments. In addition, many preclinical studies have previously used male mice for this type of model,[53–58] so this has provided the rationale for obtaining reproducible and interpretable results, creating a network of comparative data and reducing the variability related to sex differences.

The mice were randomly divided into five experimental groups, as described below:

(1) SHAM group (8): mice received saline inoculation and were orally administrated with saline;
(2) ATC group (8): mice received tumor cell inoculation and were orally administrated with saline;
(3) ATC + BITC 5 mg/kg group (8): mice received tumor cells inoculation and were orally administrated with BITC at the dose of 5 mg/kg;
(4) ATC + BITC 10 mg/kg group (8): mice received tumor cells inoculation and were orally administrated with BITC at the dose of 10 mg/kg.
(5) ATC + BITC 30 mg/kg group (8): mice received tumor cells inoculation and were orally administrated with BITC at the dose of 30 mg/kg.

METHOD DETAILS

In vitro studies

Materials

BITC was obtained from Sigma–Aldrich Company (Milan, Italy, cat. 252492). All chemicals were of the highest commercial grade available. All stock solutions were made in nonpyrogenic saline (0.9% NaCl; Baxter Healthcare Ltd., Thetford, Norfolk, UK).

Cell viability assay

Cell viability of 8305C, 8505C, ARO 81-1 BHT-101 and Nthy-0ri-3-1 cells was evaluated using a mitochondria-dependent dye for live cells (tetrazolium dye; MTT) (M5655; Sigma-Aldrich). Cells were plated on 96-well plates at a density of 4×10^4 cells/well to a final volume of 150 μl. After 24 hrs, FTC-133, K1 and 8305C cells were treated with BITC (Sigma-Aldrich®) for 24 hrs at increasing concentrations 1 μM, 10 μM, 30 μM, 50 μM, 100 μM, 200 μM and 300 μM dissolved in basal medium. After 24 hrs cell were incubated at 37°C with MTT (0.2 mg/mL) for 1 h, the medium was removed by aspiration and then cells were lysed with DMSO (100 μl). The extent of reduction of MTT to formazan was quantified by measurement of optical density at 540 nm (OD540) with a microplate reader.[59] Then, IC50 was determined by extrapolating 50% viability or inhibition to its corresponding concentration[60] (Figure S1A).

Western Blot analysis

For cell lysates, 8305C cells were washed twice with ice-cold phosphate buffered saline (PBS), collected and resuspended in lysis buffer containing 20 mM Tris-HCl pH 7.5, 10 mM NaF, 150 μl of NaCl, 1% Nonidet P-40 and protease cocktail of inhibitors (Catalog No. 11836153001; Roche, Switzerland). After 40 minutes, cell lysates were centrifuged at 12,000 rpm for 15 minutes at 4°C. Protein concentration was estimated

using the Bio-Rad protein assay (Bio-Rad Laboratories, Hercules, CA, USA) using bovine serum albumin as a standard. The samples were then heated to 95°C for 5 minutes and equal amounts of proteins were separated by 10% -15% sodium dodecyl sulfate-polyacrylamide gel electrophoresis (SDS-PAGE) and transferred to a membrane of polyvinylidene difluoride (PVDF) (Immobilon-P, catalog # 88018; ThermoFisher Scientific). The following primary antibodies were used: anti-BCL-2 (1: 500; sc-7382; Santa Cruz Biotechnology), anti-BID (1:500; sc-11423; Santa Cruz Biotechnology), anti-BAX (1:500; sc-7480; Santa Cruz Biotechnology), anti-Caspase 3 (1:500; sc-7272; Santa Cruz Biotechnology) anti-pmTOR (1:500; S2448; Cell Signaling;), anti-MAP LC3 (1:500; sc-398822; Santa Cruz Biotechnology), anti-p62 (1:500; 5114S; Cell Signaling), anti-LAMP2 (1:500; MA1-205 Invitrogen), anti-pP38 (1:500; 9211S; Cell Signaling), anti-TRAF6 (1:500; sc-7221; Santa Cruz Biotechnology). The antibody dilutions were made in PBS / 5% w / v skimmed milk powder / 0.1% Tween-20 (PMT) and the membranes were incubated overnight at 4°C. The membranes were then incubated with a secondary antibody (1: 2000; Jackson ImmunoResearch, West Grove, PA, USA) for 1 hour at room temperature. To ensure that the stains were loaded with equal amounts of protein lysate, they were also incubated with β-actin antibody (cytosolic fraction 1: 500; sc-47778; Santa Cruz Biotechnology), GAPDH (cytosolic fraction 1: 500; sc-32233; Santa Cruz Biotechnology) or laminin A/C (nuclear fraction 1: 500; sc -376248; Santa Cruz Biotechnology). We used Precision Plus protein unstained Standards (Bio-Rad 64333538) for accurate MW determination. The signals were detected with enhanced chemiluminescence (ECL) detection system mixture (Thermo Fisher, Waltham, MA, USA).[61]

Wound healing assay (Scratch test)

The effects of BITC on 8305C cell migration was performed by the Wound healing assay (Scratch test).[62] Briefly, 2 × 10^6 8305C cells were plated on 60 mm plates (Corning Cell Culture, Tewksuby, MA, USA) in a final volume of 2 ml to obtain a confluent monolayer. 24 h later, cell monolayer was scratched creating a straight line using a p200 pipette tip. After removing debris from each plate, cells were treated with increasing concentrations of BITC (30 μM, 100 μM and 200 μM) for 48 hours. In the control group, however, normal culture medium was used. Finally, to record the wound width and therefore the migratory ability of the cells, photos of each plate were acquired through a phase contrast microscope at 0, 24 and 48 hours. Cell migration rate was analyzed and calculated using Image J software.

Colony formation assay

For the colony formation assay 8305C cells were grown in six-well plates at 1,000 cells per well, and then treated with different concentrations of BITC (30 μM, 100 μM and 200 μM) or with solvent alone as a control. After 24 h of treatment, the wells were washed with PBS and incubated with RPMI-1640 medium supplemented with 10% FBS. After incubation for 10 days, the cells were washed twice with PBS and stained with 0.1% (w/v) crystal violet. The stained cells were imaged using a bright-field microscope (Zeiss).[63]

Enzyme-linked immunosorbent assay (ELISA) for IL-17 and IL-12p70

To evaluate the inflammatory response, the levels of IL-17 (ELISA kit for IL-17, SEA063Mu Cloud-Clone Corp.), IL-12p70 (Human IL-12p70 ELISA kit, KE10014, Proteintech), Cyclin A (cat ABIN6955143 Biocompare) and CDK2 (ab316258 – Human CDK2 SimpleStep ELISA Kit) were measured in cell lysates collected by enzyme-linked immunosorbent assay (ELISA), according to the manufacturer's instructions. Briefly, 100 μl of standards and cell lysates were added to the appropriate wells and incubated for 1 hour at 37°C. Then, 100 μl of 1x Detection Reagent A was added to each well and the plate was incubated for 1 hour at room 37°C. The solution was then discarded, and 4 washes were performed with 1X Wash Solution. Later 100 μl of streptavidin solution was added to each well and the plate was incubated for other 30 minutes. After repeated washes, 90 μL of Substrate Solution was added to each well and the plate was incubated for 10-20 min at 37°C protecting it from light. After adding 50 μL of Stop Solution to each well the absorbance was read immediately using microplate reader at 450 nm.

DNA fragmentation

Induction of apoptosis was analyzed by detection of DNA fragmentation performed by agarose gel electorophoresis, using the 8305C cells. Briefly 1.5 x 10^6 cells were plated and treated with BITC for 24 hours. Then the DNA was extracted using (REDExtract-N-Amp Tissue PCR Kit, XNAT-100RXN) according to the manufacturer's instructions. After electorophoresis was performed for 30 min at 100 V through 2% agarose gel. The gels were photographed under ultraviolet light.[64]

In *vivo studies*

Orthotopic model of ATC

For the orthotopic model of ATC, BALB/c-nu/nu mice will receive an injection of 5 x10^5 8305C cells, resuspended in 50 μl of saline, into the right lobe of thyroid using an insulin syringe with a 28G 1/2 needle, after anesthetizing the animals with 3% isoflurane. In detail, the human cell line 8305C was grown until 80-90% confluence was reached. Cells were then pelleted by centrifugation at 1200 rpm for 5 minutes at room temperature counted and resuspended in 50 μl of saline solution. At the same time, mouse anesthesia and surgical preparation was performed. The surgical area (from the jaw line to the top of the sternum and up to the arms) was rubbed with gauze soaked in betadine. With a sterile disposable scalpel, a 1-1.5 cm longitudinal incision was made along the midline of the throat. Next, a second incision was made in the muscle fascia surrounding the trachea and the right side of the incised muscle was pulled laterally to expose the right thyroid gland. Once the gland was exposed, 50 μl of cell suspension was slowly injected into the right thyroid gland with a with a 28G 1/2 needle insulin syringe. Then the muscle layer and skin were sutured using 6.0 suture material and a layer of triple antibiotic ointment was applied

directly to the incision site. At the end of the procedure the animals were monitored daily and weighed periodically to assess overall health (Figure S1B). 13 days later the injection, animals were treated with oral administration of BITC at different doses (5, 10 and 30 mg/kg) for 2 weeks. At the end of the experiments the animals were euthanized and thyroids and lungs harvested, weighed and analyzed.[65] In the Figure S1C we measured the volume of the tumor, using a caliper, every week starting from the inoculation carried out on day 0 until the last day of treatment on day 28. In Figure S1D, we considered the post-sacrifice weight of the entire thyroid gland to which the tumor was inoculated at the level of the right lobe.

Histological evaluation

For the histological evaluation thyroid and lungs samples were quickly removed and fixed with 10% buffered formalin for at least 24 h at room temperature. After dehydration in graded ethanol and xylene, samples were embedded in paraffin and sectioned at 7 μm thickness. After staining with hematoxylin and eosin, sections were observed by Nikon Eclipse Ci-L microscope. The histological results are shown at 10× and 20× magnification (scale bar at 100 μm and 50 μm). All histological analyses were executed in a blinded manner.[61]

Masson's trichrome staining

Morphological evaluation of tumors was performed on 5 μm sections stained using the Masson's trichrome kit (Bio-Optica cat: 04-010802), according to manufacturer instructions. The sections are hydrated following a decreasing series of alcohols and brought into distilled water. Subsequently, 6 drops of Weigert's iron hematoxylin solution were placed on the section and left to act for 10 minutes in the dark. After draining the slides, 10 drops of Picric acid alcoholic solution were added for 4 minutes. Subsequently the slides were washed quickly (3-4 seconds) in distilled water and 10 drops of Ponceau acid fuchsin according to Mallory solution were added for 4 minutes. The washing in distilled water was then repeated and the sections were stained with Phosphomolybdic acid solution for 10 minutes. After draining the slides, the Masson aniline blue solution was added and left to act for 5 minutes. Finally, the sections were washed in distilled water and rapidly dehydrated by ascending alcohols and mounted. The images were acquired using a Nikon Eclipse Ci-L microscope at the magnification of 20x (50 μm of the scale bar).[66]

Immunohistochemistry assay

Immunohistochemical localization for E-Cadherin (1:100; sc-8426 Santa Cruz Biotechnology, Dallas, TX), N-Cadherin (1:100; sc-8424 Santa Cruz Biotechnology, Dallas, TX), and S100 antibodies (1:100; sc-393919 Santa Cruz Biotechnology, Dallas, TX), was made as previously described.[67] In short, sections were incubated overnight (O/N) with the primary antibodies then were washed with PBS and incubated with secondary antibody for 1 h. The reaction was revealed using the water-soluble, chromogenic substrate 3,3′-Diaminobenzidine (DAB), and counter-stained with Nuclear Fast Red. The percentage area of immunoreactivity (determined by the number of positive pixels) was expressed as the % of total tissue area (red staining) within five random fields at an objective lens of 40 × and analyzed using a computerized image analysis system (Leica QWin V3, Cambridge, UK). The images were shown at a magnification of 20x (50 μm of the scale bar) using a Nikon Eclipse Ci-L microscope.

Western Blot analysis

Cytosolic proteins were prepared and separated electrophoretically to be transferred to nitrocellulose membranes. Membranes were blocked with 5% (w/v) dried nonfat milk in buffered saline (PM) for 45 min at room temperature and subsequently probed with specific antibodies: anti-BID (1: 500; sc-11423; Santa Cruz Biotechnology), anti-BCL-2 (1: 500; sc-7382; Santa Cruz Biotechnology), anti-BAD (1:500; sc-8044; Santa Cruz Biotechnology), anti-pmTOR (1:500; S2448; Cell Signaling), anti-p62 (1:500; 5114S; Cell Signaling), anti-PTEN (1:500; sc-7974; Santa Cruz Biotechnology) and anti-SOS1 (1:500; sc-17793; Santa Cruz Biotechnology), anti-E-Cadherin (1:100; sc-8426 Santa Cruz Biotechnology, Dallas, TX), anti-N-Cadherin (1:100; sc-8424 Santa Cruz Biotechnology, Dallas, TX), and anti-S100 antibodies (1:100; sc-393919 Santa Cruz Biotechnology, Dallas, TX), in 1× PBS, 5% w/v dried nonfat milk and 0.1% Tween-20 (PMT) at 4°C overnight. Membranes were incubated with peroxidase-conjugated goat anti-mouse IgG secondary antibody (1:2000, Jackson ImmunoResearch, West Grove, PA, USA) or peroxidase-conjugated goat anti-rabbit IgG secondary antibody (1:5000, Jackson ImmunoResearch, West Grove, PA, USA) for 1 h at room temperature. To establish that blots were loaded with equal amounts of proteins, they were also incubated in the presence of the antibody against β-actin protein (sc-8432, 1:500; Santa Cruz Biotechnology, Dallas, TX, USA). We used Precision Plus protein unstained Standards (Bio-Rad 64333538) for accurate MW determination. Signals were revealed with an enhanced chemiluminescence (ECL) detection system reagent according to the manufacturer's instructions (Thermo, Waltham, MO, USA, cat# 457). The relative expression of protein bands was quantified by densitometry with Bio-Rad ChemiDoc XRS+ software and standardized to β-actin levels as an internal control.[68]

QUANTIFICATION AND STATISTICAL ANALYSIS

Statistical analysis

All values are expressed as mean ± standard deviation (SD) of N observations. Each analysis was performed three times with three samples replicates for each one. The results were analyzed by one-way analysis of variance (ANOVA) followed by a Bonferroni post hoc test for multiple comparisons. A value of $p < 0.05$ was considered significant.

Principal component analysis (PCA)

Principal component analysis (PCA) was used to plot the vector network obtained by analyzing the correlation coefficient data matrix (Figures S2 and S3). In the graphs obtained, the angle between the vectors is inversely proportional to the degree of correlation between the vectors; The same direction of the vector indicates a positive correlation/covariance, the direction of the opposite vector indicates a negative correlation/covariance. This allows a visualization of the situation under study and is an excellent method to grasp meaning from systems biology assessments.[69] The PCA plot is based on the differential expression analysis with the R package "stats". We used R (version 4.4.0), including tidyverse and ggfortify packages, to perform PCA. To prepare the data for PCA, we used the prcomp function in centering and scaling mode, which ensured that each variable had an equal effect on the analysis. R-squared was calculated to quantify how much variance each principal component explains. A biplot was created by utilizing the autoplot function of package ggfortify with additional parameters for variable display.